Tectonic and oceanographic process interactions archived in the Late Cretaceous to Present deep-marine stratigraphy on the Exmouth Plateau, offshore NW Australia

Running title: Tectonic and oceanographic history NW Australia

Harya D. Nugraha
Basins Research Group (BRG), Department of Earth Science and Engineering, Imperial College, Prince Consort Road, London SW7 2BP, UK
Tel: +44(0)7491 475 075
harya.nugraha14@imperial.ac.uk

Department of Geological Engineering, Universitas Pertamina, Jalan Teuku Nyak Arief, Jakarta 12220, Indonesia

Christopher A-L. Jackson
Basins Research Group (BRG), Department of Earth Science and Engineering, Imperial College, Prince Consort Road, London SW7 2BP, UK
Tel: +44(0)20 7594 7450
c.jackson@imperial.ac.uk

Howard D. Johnson
Basins Research Group (BRG), Department of Earth Science and Engineering, Imperial College, Prince Consort Road, London SW7 2BP, UK
Tel: +44(0)20 7594 6450
h.d.johnson@imperial.ac.uk

David M. Hodgson
Stratigraphy Group, School of Earth and Environment, University of Leeds, Leeds LS2 9JT, UK
Tel: +44(0)113 343 0236
d.hodgson@leeds.ac.uk

Matthew T. Reeve
Basins Research Group (BRG), Department of Earth Science and Engineering, Imperial College, Prince Consort Road, London SW7 2BP, UK
Tel: +44(0)7986 643 635
matthew.reeve09@imperial.ac.uk

Corresponding Author

Harya D. Nugraha

harya.nugraha14@imperial.ac.uk

ABSTRACT

Deep-marine deposits provide a valuable archive of process interactions between sediment gravity flows, pelagic sedimentation, and thermo-haline bottom-currents. Stratigraphic successions can also record plate-scale tectonic processes (e.g. continental breakup and shortening) that impact long-term ocean circulation patterns, including changes in climate and biodiversity. One such setting is the Exmouth Plateau, offshore NW Australia, which has been a relatively stable, fine-grained carbonate-dominated continental margin from the Late Cretaceous to Present. We combine extensive 2D (~40,000 km) and 3D (3,627 km^2) seismic reflection data with lithologic and biostratigraphic information from wells to reconstruct the tectonic and oceanographic evolution of this margin. We identified three large-scale seismic units (SUs): (1) SU-1 (Late Cretaceous) – 500 m-thick, and characterised by NE-SW-trending, slope-normal elongate depocentres (c. 200 km long and 70 km wide), with erosional surfaces at their bases and tops, which are interpreted as the result of contour-parallel bottom-currents, coeval with the onset of opening of the Southern Ocean; (2) SU-2 (Palaeocene – Late Miocene) – 800 m-thick and characterised by: (i) very large (amplitude, c. 40 m and wavelength, c. 3 km), SW-migrating, NW-SE-trending sediment waves, (ii) large (4 km-wide, 100 m-deep), NE-trending scours that flank the sediment waves, and (iii) NW-trending, 4 km wide and 80 m deep turbidite channel, infilled by NE-dipping reflectors, which together may reflect an intensification of NE-flowing bottom currents during a relative sea-level fall following the establishment of circumpolar-ocean current around Antarctica; and (3) SU-3 (Late Miocene – Present) – 1000 m-thick and is dominated by large (up to 100 km^3) mass-transport complexes (MTCs) derived from the continental margin (to the east) and the Exmouth Plateau Arch (to the west), and accumulated mainly in the adjacent Kangaroo Syncline. This change in depositional style may be linked to tectonically-induced seabed tilting and folding caused by collision and subduction along the northern margin of the Australian plate. Hence, the stratigraphic record of the Exmouth Plateau provides a rich archive of plate-scale regional geological events occurring along the distant southern (2000 km away) and northern (1500 km away) margins of the Australian plate.

Keywords: Tectonics and sedimentation, palaeo-oceanography, deep marine, seismic reflection, bottom current, contourites, MTCs, Exmouth Plateau, NW Australia.

1. Introduction

Sedimentary successions in deep-marine basins record process interactions between down-slope (e.g. gravity-driven sediment transport processes) and along-slope processes (e.g. thermohaline bottom-current circulation), in addition to *in-situ* (hemi)pelagic sedimentation, (e.g. Stow & Piper, 1984; Pickering *et al.*, 1989; Huneke & Mulder, 2010; Llave *et al.*, 2018). One of these processes may dominate, both spatially and temporally, for instance, periods of intense tectonism may be recorded by repeated deposition of mass-transport complexes (MTCs) spatially associated with specific structures (Hampton *et al.*, 1996; Bagguley & Prosser, 1999; Gee *et al.*, 2006; Gee *et al.*, 2007; Masson *et al.*, 2010; Ortiz-Karpf *et al.*, 2016; Pérez *et al.*, 2016; Scarselli *et al.*, 2016). In contrast, periods dominated by the activity of intense, along-slope bottom currents may be recorded by deposition of contourite depositional systems, from which oceanographic and/or palaeo-oceanographic processes can be inferred (Pickering *et al.*, 1989; Viana *et al.*, 1998; Hernández-Molina *et al.*, 2006b; Uenzelmann-Neben, 2006; Ercilla *et al.*, 2016; Hernández-Molina *et al.*, 2016; Pérez *et al.*, 2017). Therefore, deep-marine stratigraphy can record tectonic and oceanographic processes, including periods of continental rifting and collision that may result in the opening and closing of ocean gateways (Faugères & Stow, 1993; Knutz, 2008; Hernández-Molina *et al.*, 2016; Pérez *et al.*, 2017).

To date, bottom-current deposits (i.e. contourites) have been used as proxies to reconstruct: (i) the history of palaeo-oceanographic and/or palaeoclimatic changes (e.g. Mulder *et al.*, 2002; Uenzelmann-Neben, 2002; Hernández-Molina *et al.*, 2006a; Uenzelmann-Neben & Gohl, 2012; Vandorpe *et al.*, 2014; Gruetzner & Uenzelmann-Neben, 2016; Pérez *et al.*, 2017); and (ii) the contribution of oceanographic processes on continental margins and deep-marine basins evolution (e.g.Johnson & Damuth, 1979; Reed *et al.*, 1987; Hernández-Molina *et al.*, 2006b; García *et al.*,

2009a; Zhu *et al.*, 2010; Martos *et al.*, 2013; Pérez *et al.*, 2014; Soares *et al.*, 2014; Pérez *et al.*, 2017). On the other hand, the timing and distribution of gravity-driven deposition has been used to reconstruct the tectono-sedimentary evolution of passive (e.g. Heinio & Davies, 2006; Gamboa *et al.*, 2010; Clark *et al.*, 2012; Armandita *et al.*, 2015; Scarselli *et al.*, 2016; Thöle *et al.*, 2016), and active margins (e.g. Normark *et al.*, 2006; Romans *et al.*, 2009; Schwenk & Spieß, 2009; Romero-Otero *et al.*, 2010; Vinnels *et al.*, 2010; Covault *et al.*, 2011; Richardson *et al.*, 2011; Sømme *et al.*, 2011; Völker *et al.*, 2012; Alfaro & Holz, 2014; Pérez *et al.*, 2016). In addition, process interactions between these along- and downslope processes have also been documented (e.g. Kähler & Stow, 1998; Michels *et al.*, 2001; Akhurst *et al.*, 2002; Mulder *et al.*, 2006; Salles *et al.*, 2010). For example, not only can bottom-currents rework gravity-driven deposits (e.g. Shanmugam, 2003; Marchès *et al.*, 2010), but they also can destabilise a slope and eventually trigger gravity-driven processes (e.g. Esmerode *et al.*, 2008; Martorelli *et al.*, 2016). However, the way in which the deep-marine stratigraphy of relatively stable passive margins (i.e. without salt or mud tectonics) records the evolution of tectonic and oceanographic process interactions along distant (>1000 km) plate-tectonic margins remains an important problem to address.

The Late Cretaceous to Present successions of Exmouth Plateau provides an opportunity to examine how deep-marine stratigraphy archives plate-scale tectonic and oceanographic events, since it is located between areas of seafloor spreading to the south (Australian-Antarctic rift) and continental collision to the north (Australia-Eurasia subduction zone). The Exmouth Plateau is a continental block on the north-western Australian continental margin (Fig. 1a), which has been a carbonate-dominated deep-marine basin since the Late Cretaceous (Fig. 2) (Exon *et al.*, 1992; Haq *et al.*, 1992). Although the regional tectonic development of the Exmouth Plateau and surrounding areas is well-documented (Karner & Driscoll, 1999; Cathro & Karner, 2006; Keep *et al.*, 2007; Müller *et al.*, 2012), the sedimentary processes operating during the late post-rift megasequence (i.e. Late Cretaceous to Present) remain poorly-understood, mainly due to their low hydrocarbon potential. We here use a

high-quality, extensive (cumulative length of ~40.000 km) time-migrated 2D seismic reflection dataset to: (i) define regional basin structure; (ii) characterise depocentre style and migration resulting from, and recording, a range of tectonic events; (iii) infer depositional style via seismic facies analysis; and (iv) document interaction of down- and alongslope depositional processes. In addition, a time-migrated 3D seismic reflection volume (3627 km^2) is used to understand erosional and depositional processes in a more complex area. We also use well data to constrain lithology, age, and palaeo-water depth.

We demonstrate that the offshore seismic stratigraphy provides a proven record of tectonic and oceanographic process interactions. The deep-marine stratigraphy of the Exmouth Plateau are: (i) dominated by bottom-current deposits and associated erosional features from the Late Cretaceous to late Miocene; and (ii) dominated by the emplacement of MTCs since the late Miocene. The former is linked to rifting and the opening of ocean gateway along the southern margin of the continent, and the latter is related to a collision and the closing of ocean gateway along the northern margin of the continent.

2. Geological setting

2.1 Tectonostratigraphic framework

The Exmouth Plateau is located between upper and lower slopes of the northwest Australia continental margin (Falvey & Veevers, 1974), in water depths ranging from 800 to 4000 m (Exon *et al.*, 1992). The plateau is bound by continental shelf to the southeast, and the Argo, Gascoyne and Cuvier abyssal plains to the northeast, northwest and southwest, respectively (Longley *et al.*, 2002) (Fig. 1a). The Exmouth Plateau is a sub-basin of the North Carnarvon Basin, which underwent multiple rifting events between the Late Carboniferous and Early Cretaceous, with seafloor spreading commencing in the Argo Abyssal Plain in the Late Jurassic and in the Gascoyne and Cuvier abyssal plains in the Early Cretaceous (Tindale *et al.*, 1998; Longley *et al.*, 2002) (Fig. 1a-b).

This study focuses on the late post-rift megasequence (Fig. 2), which is Late Cretaceous to Present-day in age, and is defined, on the Exmouth Plateau at least, by the sustained deposition of fine-grained carbonates (i.e. chalk and oozes) as recorded in Ocean Drilling Program (ODP) 762 and 763 cores (Figs 1b and 2) (Haq *et al.*, 1992; Boyd *et al.*, 1993). An unconformity defining the Cretaceous-Palaeogene boundary (Boyd *et al.*, 1993) most probably formed by enhanced bottom-current erosion (Fig. 2) (Haq *et al.*, 1992) related to the change of primary seafloor spreading axis from the Indian to the Southern Ocean (Fig. 2) (Baillie *et al.*, 1994). At the start of the Oligocene, a global eustatic sea level fall occurred as a result of continental ice sheet build-up in Antarctica (Miller *et al.*, 1991). Oligocene to late Miocene sediments are the thickest beneath the present shelf where they are represented by a progradational, clinoform-bearing carbonate succession; further basinward, on the Exmouth Plateau, this interval is represented by a thin pelagic succession (Tindale *et al.*, 1998). Another unconformity defining the base of the late Miocene to Present succession most probably record collision between Australia and Eurasia (Boyd *et al.*, 1993; Hull & Griffiths, 2002). The late Miocene to Present succession thickens further basinward and onlaps the underlying sediments on the shelf (Fig. 3), suggesting accelerated tectonic subsidence on the Exmouth Plateau associated with inverted pre-existing faults beneath the present shelf (Fig. 2) (Hull & Griffiths, 2002). The collision is variably expressed along the Northwest Shelf of Australia (e.g. the Exmouth Plateau Arch), which is controlled by the orientation between the regional compressional stress field and pre-existing, rift-related structures (Keep *et al.*, 1998). On the Exmouth Plateau, broad folding of the Exmouth Plateau Arch about an NE-SW axis led to gravity-driven sediment transport resulting in deposition of MTCs, with sediments being thin on the plateau crest and thick in the adjacent Kangaroo Syncline (see Fig. 3) (Boyd *et al.*, 1993).

2.2 Present-day oceanographic setting

Two currents dominate the present-day ocean circulation offshore NW Australia (Fig. 1a) (e.g. Wells & Wells, 1994): (i) the poleward-flowing Leeuwin Current (LC) and (ii) the equatorward-flowing

Western Australian Current (WAC) (Fig. 1a). Most ocean basins in the southern hemisphere are dominated by an anti-clockwise gyre, which results in an Eastern Boundary Current that flows northward to the equator along continental margins (e.g. Benguela Current, offshore southern Africa, and the Humboldt Current, offshore Peru and Chile) (Collins *et al.*, 2014). The Northwest Shelf of Australia is dominated by the southward-flowing Leeuwin Current rather than the Eastern Boundary Current (i.e. the WAC) (Fig. 1a). The Leeuwin Current is a low-salinity, nutrient-poor, narrow (<100 km wide), high velocity current (0.1 to 0.4 m/s), flowing down to 300 m water depth (James *et al.*, 2004). It is sufficiently energetic (Pearce, 1991) to form depositional bedforms within sand-sized sediments (Stow *et al.*, 2009). The LC flows as a result of strong trade winds in the equator that push the westward-flowing South Equatorial Current (SEC) through Indonesia (Indonesia Throughflow, ITF) (Fig. 1a) (Collins *et al.*, 2014). The SEC induces a pressure-gradient in the eastern Indian Ocean that forces warm surface water to flow southward along the western shelf of Australia, i.e. the Leeuwin Current (Smith *et al.*, 1991). The other current, the WAC (Fig. 1a), is a cold, high-salinity, nutrient-rich current (Spooner *et al.*, 2011), which influences water masses as deep as 2000 m (Tchernia, 1980). The Leeuwin Undercurrent (LU) (Haller et al., 2018), which forms part of the WAC, is a high velocity current (0.32 to 0.4 m/s) with its core at a depth of 400 m (Fig. 1a) (Woo & Pattiaratchi, 2008). The LU is interpreted as a prolongation of Flinders Current that flows along southern margin of Australia (Woo & Pattiaratchi, 2008). However, the FC is not the only source for the LU, which is also fed by the southern South Indian Counter Current (SICC) near its northern end (Fig. 1a) (Wijeratne *et al.*, 2018).

3. Data set and methodology

3.1 Data set

We use two types of seismic reflection data (see Fig. 1b and Table S1), provided by Geoscience Australia: (i) 412 2D data lines with a cumulative line length of ~40,000 km, covering an area of ~109,000 km^2. These data were collected between 1993 and 2005, with the dominant frequency

ranging from 30 to 50 Hz in the interval of interest, and (ii) a 3D seismic volume (Duyfken 3D MSS, acquired in 2006) that covers an area of 3627 km^2, with a bin size of 18.75 x 12.5 m (i.e. inline x crossline) and a dominant frequency of 50 Hz in the interval of interest (Fig. 1b). Given an average velocity of 2000 m/s derived from checkshot data from wells (see Fig. 3 for location), we estimate the vertical resolution ($\lambda/4$) of the seismic data ranges from 10 – 17 m for the 2D data, and is c. 10 m for the 3D data. Seismic reflection data polarity follows SEG normal convention (Brown, 2011), where a downward increase of acoustic impedance manifests as a negative reflection event (trough), and a downward decrease of acoustic impedance manifests as a positive reflection event (peak).

This study uses 12 wells that provide lithological and well-log (Table S2 and S3), biostratigraphic (Table S4 and Fig. S1), palaeo-water depth (Fig. S2 and S3), and velocity (Fig. S4) data within the study interval. These wells are chosen based on their spatial distribution (i.e. in an area where several wells are clustered, only the well with the most complete data was chosen). The study interval is not a primary petroleum exploration target, therefore borehole data (e.g. lithological, biostratigraphic, and well-log) is rather sparse (see Tables S2-S4 and Figs S1-S2). Industry wells provide lithology data based on ditch cuttings, with conventional core data provided by two ODP Leg 122 wells (ODP 762 and 763). Most well-logs terminate below or within the lower part of the study interval, and only GR (gamma-ray) logs sample the majority of the study interval. Of the 12 wells, five contain biostratigraphic data within the study interval. These wells were utilised to constrain the age of interpreted surfaces from seismic reflection data, and biostratigraphic data provided palaeo-water depth estimations (Fig. S2). However, because palaeo-water depth data are scarce in the upper part of the study interval, we infer the palaeo-water depth based on the height of Oligocene to Present clinoforms (see Hull & Griffiths, 2002) (Fig. 2). Velocity data from checkshots were used to convert seismic interpretation deliverables (e.g. time-structure maps) from the time domain in milliseconds two-way time (ms TWT) to the depth domain in meters by using 2^{nd}-order polynomial best-fit line equation (Fig. S4).

3.2 Methodology

3.2.1 Seismic-stratigraphic framework

Exon and Willcox (1980) conducted the earliest seismic reflection-based investigations of the Exmouth Plateau. Following drilling of ODP Leg 122 wells (i.e. ODP 762 and 763), Boyd *et al.* (1993) updated previous interpretations, providing better lithology and age constraints on the penetrated succession. Our study recognises four regionally significant horizons (Figs 2 and 3) previously identified by Boyd *et al.* (1993). These horizons were interpreted based on seismic-stratigraphic relationships (i.e. truncation, onlap, and downlap), and vertical and lateral variations of internal seismic reflection geometry. We identify four seismic facies (see Fig. 5): (i) SF-1 - continuous, sub-parallel reflections; (ii) SF-2 - sub-parallel with internal truncation reflections; (iii) SF-3 - sub-parallel to wavy reflections; and (iv) SF-4 - discontinuous to chaotic reflections. The interpreted horizons (from bottom to top; i.e. Horizon A-D) define three seismic units (Figs 2 and 3): (i) SU-1 – Late Cretaceous, equivalent to Package 6 of Boyd *et al.* (1993); (ii) SU-2 – Palaeocene-late Miocene, equivalent to Package 7 of Boyd *et al.* (1993); and (iii) SU-3 – late Miocene-Present, equivalent to Package 8 of Boyd *et al.* (1993). We mapped five additional horizons within SU-2 within the 3D seismic dataset (Fig. 2); these relatively high-amplitude, continuous seismic reflections horizons, which are only locally mappable, define vertical changes in seismic facies and, we infer, depositional locus and process. However, only three of them (i.e. Horizon C-2, C-3, and C-4) are discussed further here (Section 4.2), as they provide the most significant evidence to interpret palaeo-oceanographic processes. Seismic attributes, such as RMS amplitude and variance (see Text S1 for explanation), were extracted from the 3D seismic reflection data to aid interpretation and to augment conventional seismic mapping (Brown, 2011).

3.2.2 Borehole data interpretation

Several wells provide lithologic control on the studied succession. ODP 762 and 763 wells contain conventional core throughout the study interval, with other wells yielding ditch cuttings (Table S2, see Fig. 4). The age of seismic surfaces are constrained by biostratigraphic data (Table S4 and Fig.

S1); in this study we used a planktonic foraminifera-based biozonation scheme, as the associated data are consistently available in all five wells containing biostratigraphic data. In addition, we also incorporated palaeo-water depth data derived from several wells, based on planktonic-foraminifera (i.e. Eskdale-1, Orthrus-2, Mercury-1, ODP 762 and 763, see Fig. S2). Note that we refer to biozonation scheme of Kelman *et al.* (2013) and the geological timescale of Gradstein *et al.* (2012).

4. Results

4.1 SU-1 (Late Cretaceous)

SU-1 is bound by Horizon A and B at the base and top, respectively. SU-1 is composed of carbonate-dominated sediments (i.e. marl and chalk), which overlie clay-dominated, siliciclastic sediments (Fig. 4). Horizon A therefore marks the transition from a clastic- to carbonate-dominated depositional regime. Biostratigraphic data (Fig. S1) show that the Horizon A defines the Cenomanian/Turonian boundary (~93.9 Ma) (*cf.* Reflector 5 of Boyd et al., 1993).

4.1.1 Basal surface: Horizon A

Horizon A defines the base of the studied interval. It truncates underlying seismic reflections, most notably along the axis of the Kangaroo Syncline axis (e.g. Figs 6a and c); elsewhere, it is generally conformable (e.g. Figs 6f and h).

Four elongate, at least 7.5 km-long and 3 km-wide sedimentary bodies, oriented sub-parallel to the present, NE-trending slope are observed on Horizon A ('pre-SU-1 mounds'; outlined in red in Fig. 7b). These bodies are defined by sub-parallel, continuous, reflections in their lower part, and are mounded in their upper part (Figs 6a, c-d).

The 3D seismic data imaged one of the pre-SU-1 mounds, where Horizon A displays significant relief of at least 500 m (Figs 6a and 8a). An RMS amplitude map of Horizon A reveals a suite of predominantly NE-trending amplitude anomalies are developed on top of the pre-SU-1 mounds (Fig.

8b). These anomalies are: (i) sinuous lineations corresponding to truncation of underlying reflections (Fig. 8c), and (ii) straight lineations defining U-shaped depressions (c. 2.5 km-wide and c. 100 m-deep) (Fig. 8d).

4.1.2 Characteristics of SU-1

Due to erosion along Horizon B (described in Section 4.21), SU-1 varies in thickness (e.g. Figs 6b-d). Major (up to 600 m thick) SU-1 depocentres are located along the Kangaroo Syncline, where they are c. 200 km-long and 70 km-wide, and trend NE, sub-parallel to the present slope (Fig. 7c). Between these elongate depocenters, SU-1 is relatively thin and has a channel-like form (Figs 6b-c) shaped by Horizon B, that incises down to 250 m. Elsewhere, such as in the northern and western part of the study area, SU-1 has a broadly uniform thickness (c. 250 m), progressively thinning southward (Fig. 6e) and westward (Fig. 6f).

Although SU-1 is dominated by SF-1 (Figs 6b and 7c), internal seismic facies variations occur. For example, a NE-trending, channel-like seismic facies (i.e. SF-2, see Fig. 5) occur along the Kangaroo Syncline (Figs 6b-c and 7c). The 3D seismic data partly imaged this feature, showing it corresponds to the sinuous lineations in Figs 8a-c.

4.1.3 Interpretation of SU-1

Prior to SU-1 deposition, the Exmouth Plateau had been in an outer-shelf (Boyd *et al.,* 1993) or deep-marine (Young *et al.,* 2001) environment, an interpretation confirmed by the existence of a NE-trending shelf-edge located along the present-day Resolution Arch (Young *et al.,* 2001; Boyd *et al.,*1993) (see Fig. 7a). Beneath Horizon A, a progressive change of seismic facies within the pre-SU-1 mounds, from sub-horizontal in the lower part to more mounded upwards (Figs 6a and c-d), resembles a classic mounded drift development (e.g. Faugères *et al.*, 1999). The truncation of reflections at the top of the pre-SU-1 mounds by Horizon A (Figs 6a and c-d) indicate a major erosional event following construction of the mounded drifts. We therefore interpret both

283 constructional and erosional processes controlled development of pre-SU-1 mounds. In addition,
284 their elongate geometry, in particular their orientation sub-parallel to the NE-trending present slope
285 (Fig. 7b), is consistent with an origin as contourite drifts (e.g. Rebesco *et al.*, 2014). Pre-SU-1 mounds
286 were previously interpreted by Romine *et al.* (1997) and Young *et al.* (2001) as Albian contourites.
287 However, their limited seismic coverage did not allow them to infer the direction of the causal
288 current.

289 SU-1 was deposited from the Turonian (~93.9 Ma) to the Maastrichtian (~66 Ma). It was deposited in
290 relatively deep-marine environment (>200 m), an interpretation supported by palaeo-water depth
291 data from: (i) wells (Fig. S4), which indicate at least upper neritic to bathyal depths (100-500 m); (ii)
292 biostratigraphic data from Hull and Griffiths (2002), which indicate water depths of 200-1000 m in
293 Rankin Platform and Dampier Sub-basin (Fig. 1b); and (iii) Boyd *et al.* (1993), who suggest that, based
294 on the topographic relief of the Pre-SU-1 interval (their Package 5), suggest the palaeo-water depth
295 at this time was at least 300 m.

296 Pelagic or hemipelagic deposition dominated during deposition SU-1 (i.e. SF-1; e.g. Figs 6b-c and e).
297 An alternative interpretation, based on their tabular-to-low-relief mounded geometries, and their
298 mid-slope position, is these seismic packages represent slope sheeted drifts (Faugères *et al.*, 1999;
299 Hernández-Molina *et al.*, 2008). In addition to SF-1, additional erosional features are observed in SU-
300 1 (i.e. SF-2). When interpreting these bottom current-related erosional features, we follow the
301 classification of Hernández-Molina *et al.* (2008) and García *et al.* (2009b), where: (i) *contourite*
302 *channels* trend along-slope, sinuous, or oblique relative to the slope and have deeply erosional bases
303 formed mainly due to the action of bottom currents; (ii) *moats* are along-slope trending with
304 erosional base, channel-shaped features that are genetically-related to elongated mounded drift,
305 and formed initially by non-deposition and local erosion beneath bottom currents' core, controlled
306 by Coriolis force; (iii) *scours* are linear erosional features generated because of the effects of
307 bathymetric obstacles; and (iv) *furrows*, which are smaller and less erosional than contourite

channels, formed by small current that is detached from the main bottom current. Therefore, based on: (i) slope-normal orientation, (ii) contained seismic facies, and (iii) their spatial relationship to other features inferred to form due to the activity of bottom currents, we interpret the channel-like seismic facies of SU-1 (i.e. SF-2; e.g. Figs 6b-c) as contourite channels. These SU-1 contourite channels trend perpendicular to coeval, NW-trending incised canyons; bottom current-reworked canyon fills are identified adjacent to the Resolution Arch (see Fig. 7a) (Young *et al.*, 2001).

The 3D seismic reflection data image evidence for the action of bottom currents, including: (i) the sinuous lineations interpreted as contourite channels (Figs 7c and 8b-c); and (ii) straight, U-shaped lineations interpreted as furrows (Figs 8b and d). We did not interpret the latter as gullies (*cf.* Lonergan *et al.*, 2013), because these features are: (i) normal rather than parallel to the slope; (ii) significantly larger (as compared to gullies in that study, which are only 160-625 m-wide and 8-43 m-deep), and (iii) not regularly-spaced.

4.2 SU-2 (Early Palaeocene-Late Miocene)

SU-2 is bound by Horizon B and C at the base and top, respectively. SU-2 is composed of calcarenite and calcilutite along the shelf, and pelagic chalk further north-westward on the Exmouth Plateau (Fig. 4). Biostratigraphic data (Fig. S1) show that the Horizon B defines Cretaceous/Palaeogene boundary (~66 Ma) (*cf.* Reflector 6 of Boyd *et al.*, 1993).

4.2.1 Basal surface: Horizon B

Horizon B can be traced across much of the study area. It is generally characterised by a high-amplitude, continuous, negative reflection that is commonly offset by low-displacement normal faults (e.g. Fig. 6b). As previously discussed, Horizon B truncates SU-1, defining the prominent SU-2 contourite channel (Figs 7c-d). Highly irregular relief (c. 200 m) produced by this horizon is located within an area termed as the 'V-shaped facies zone' (VFZ) (Figs 6d and 7d); this is discussed in detail later in this section.

4.2.2 Characteristics of SU-2

Thickness patterns in SU-2 defines a marked shift in the locus of deposition (Fig. 7d), most notably around the Exmouth Plateau Arch. Here, SU-2 thins south-westward (from 500 m to 200 m, Fig. 6e) and thickens (c. 450 m) westward (Fig. 6f); this contrasts with SU-1, which was progressively thinning westward.

SU-2 contains three distinctive seismic facies (see Fig. 7d): (i) SF-1 dominates (e.g. Figs 6e and h), with sub-horizontal and NE-dipping variants observed (Fig. 6a); (ii) SF-2, which is best-developed along the axis of the SU-2 contourite channel (Figs 6b-c); and (iii) SF-3, which is best-developed within the VFZ, and is imaged in the NE of the 3D dataset (Figs 6a, d and 7d). The detailed geometry of the VFZ is difficult to interpret in 2D seismic reflection data due to the relatively low resolution of these data, and the inherent stratigraphic complexities of this part of SU-2 (see Horizon C-4 in Fig. 6d). We therefore mapped five local horizons (i.e. C-1 to C-5) in the 3D seismic reflection data that allow us to better understand the transition from an area where relatively simple, NE-dipping reflections of SF-1, to the more complex VFZ (e.g. Figs 6a and 7d).

The interval between B and C-1 is dominated by sub-parallel reflections that are offset by low-displacement normal faults (SF-1) (Fig. 9a). The overlying interval (C-1 to C-2) is composed of continuous wavy reflections above the pre-SU-1 mound slope, changing laterally into discontinuous but locally wavy reflections to the NE (Fig. 9a). The wavy reflections along C-2 have a maximum amplitude of 40 m, with the wavelength between two troughs being up to 3 km. Wave crests trend NNW and can be traced for up to ~12 km (Fig. 9b). Between C-2 and C-3, the wave crests migrate south-westward by ~1 km (Fig. 9a-c), with wave amplitude and wavelength on C-3 being similar to that on C-2. However, C-3 truncates C-2 above the pre-SU-1 mound at the base-of-slope (Fig. 9a), forming predominantly NE-trending channels on the NW and SE sides of the waves (Fig. 9c). Between C-3 and C-4, waves migrate a further c. 500 m to the SW (Figs 9a, c-d), with local

preservation of the 3 km wide, 100 m deep scours previously formed along Horizon C-3 (Fig. 9d). These horizons also reveal a 4 km wide and 80 m deep channel that trends NW; this channel is broadly perpendicular to, but is physically connected with, the channels developed on the sides of the sediment waves (Fig. 9c-d and Fig. 10). Lineations up to 10 km-long, 5-20 m-deep, and 60-150 m-wide occur on the base of scours developed along C-4 (Figs 9d and 10). The interval between C-4 and C is predominantly composed of sub-parallel reflections, with an erosional surface (C-5) in between.

4.2.3 Interpretation of SU-2

SU-2 was deposited from the Palaeocene (~66 Ma) until the late Miocene (~9 Ma). Biostratigraphic data from Orhtrus-1 (see Fig. 1b) indicate the palaeo-water depth at the beginning of SU-2 deposition was at least 200 m. Young *et al.* (2001) estimate palaeo-water depth on the plateau was initially c. 200 m and progressively increased to c. 1100 m at the end of SU-2. Together, these data imply that SU-2 deposition was deeper than that of SU-1. In addition, the trend of the continental margin (i.e. NE-trending) during this time was similar to that of earlier periods (e.g. Boyd *et al.*, 1993; Young *et al.*, 2001; Hull & Griffiths, 2002), with NW-prograding, carbonate-dominated clinoforms observed along the SE basin margin (see Fig. 3).

Thickness variations in SU-2 reflect growth of the Exmouth Plateau Arch. Folding of the arch may have occurred after deposition of SU-2, an interpretation supported by truncation of reflections within SU-2 by Horizon C (Figs 6f-g), and the apparent lack of true depositional thinning onto the arch crest. In this case, thickness changes in SU-2 are primarily driven by erosion at its top, with this being greatest near the arch crest. In addition, SU-2 thickens westwards as a result of post-breakup subsidence of the western margin of the plateau, coupled with growth of the Exmouth Plateau Arch; this contrast with the eastward-thickening observed in SU-1 (Fig. 6f).

Although SU-2 is dominated by pelagic and hemipelagic deposition (SF-1), bottom current activity is evident by the SU-2 contourite channel and additional erosional features within the VFZ (Fig. 7d).

SU-2 filled accommodation created by Horizon B, suggesting bottom current strength decreased with time (e.g. Faugères & Stow, 2008).

At least three processes might be responsible for the complex geometry observed in VFZ (see Fig. 9a): (i) gas hydrate dissociation; (ii) downslope processes; and (iii) alongslope processes. Imbert and Ho (2012) interpret the V-shaped features as fossil hydrate pockmarks (i.e. collapsed pockmarks) initiated by methane hydrate emplacement along conical failures originating from the subsurface to Palaeocene-Eocene seabed. The emplaced methane hydrate was then dissociated, driving formation of collapsed pockmarks. However, the trigger for gas hydrate dissociation on the Exmouth Plateau is inferred to be a relatively rapid increase in ocean temperatures during the PETM (i.e. Palaeocene-Eocene Thermal Maximum) (Imbert and Ho, 2012). The PETM is a major global hyperthermal event resulting from methane release caused by rapid hydrocarbon source rock maturation induced by rift-related magmatism in the north Atlantic Ocean (Svensen *et al.*, 2004). We propose that the gas hydrate dissociation mechanism, although potentially important, is not the only mechanism that could have formed the complex features in the VFZ.

Down- and alongslope processes may have controlled formation of the complex geometries observed in the VFZ. The planview geometry of the C-3 and C-4 channels is tributive (see Figs 9c-d), with the NE-trending, slope-normal channels (possibly controlled by local relief across the pre-SU-1 mound) feeding the NW-trending, slope-parallel channel (Fig. 10). Thus, erosion related to the action of turbidity currents may have played a role in the formation of the VFZ. However, it is unlikely that the NE-trending channels formed by turbidity currents as they are oriented alongslope (see Fig. 9c-d). Reactivation of pre-existing faults beneath the shelf during this time (Young *et al.*, 2001) could eventually, however, have generated turbidity currents and formed the downslope-oriented, NW-trending channel.

We suggest that alongslope processes drove formation of the VFZ. The NE-dipping reflections (Fig. 6a) are interpreted to be a down-current migrating (to the NE), slope sheeted contourite drift (Faugères *et al.*, 1999) (Fig. 6c). This drift passes north-eastward into large (*sensu* Symons *et al.*, 2016; Hofstra *et al.*, 2018), fine-grained (*sensu* Wynn & Stow, 2002) sediment waves that define the VFZ. We suggest these sediment waves formed in response to bottom current activity, as opposed to turbidity currents, because of their close temporal and spatial relationship with the sheeted contourite drift. Sediment waves continued to grow and migrate to the SW up to C-4 (Fig. 10a). We infer bottom currents flowed towards the NE-ENE, as bottom current direction is generally perpendicular (Flood, 1988) or oblique (Blumsack & Weatherly, 1989) to sediment wave crests (Fig. 9b).

The presence of NE-trending channels that first developed at C-3 and continued up to C-4 imply the sediment waves became an obstacle to bottom current flow, resulting in flow separation and subsequent erosion on the marginal sides of the obstacle (e.g. Hernández-Molina *et al.*, 2006a). Due to their genetic relation to the obstacle, the NE-trending channels are called *scours* (see Section 4.1.3). Discontinuous wavy reflections on the down-current side of the large sediment waves are interpreted as depositional 'tails' developed as a result of complex flow interactions and decreasing flow velocities behind the obstacle (Figs 9c-d) (Davies & Laughton, 1972; Hernández-Molina *et al.*, 2006a). We infer that the NE-flowing 'palaeo-WAC' formed the sediment waves and scours. In contrast, the NW-trending channel is unlikely to have a bottom current origin, and most likely to be formed by the action of turbidity currents. An example of bottom current-related downslope trending features is Blake-Bahama drift, western North Atlantic (Faugères *et al.*, 1999) resulting from interaction of two opposing, near-surface and deep bottom currents. However, this drift is a depositional not erosional feature. Therefore, although the WAC has been operating and the LC might have been formed due to northward drift of Australia during this time (i.e. since late middle Eocene, see Fig. 2) (McGowran *et al.*, 1997), they were unlikely to form the NW-trending channel.

Lineations at the base of the scours and the channel (C-4; Figs 9d and 10a-b) might be the result of erosion by turbidity currents (i.e. large tool marks) or bottom currents due to their orientations and small dimensions (i.e. furrows, e.g. Stow *et al.*, 2009).

Hence, it is proposed that both down- and alongslope processes, in addition to potential gas hydrate dissociation, are responsible for formation of the VFZ. Interaction between the downslope (i.e. turbidity currents) and alongslope (i.e. palaeo-WAC) processes is documented within the NW-trending channel; where it is infilled with sediments dipping to the NE (i.e. the same direction of the palaeo-WAC; Fig. 10a-b). This type of interaction is also documented elsewhere (e.g. South China Sea; Zhu et al., 2010; and SE Brazilian margin; e.g. Faugères et al., 1999).

4.3 SU-3 (Late Miocene-Present)

SU-3 is bound by Horizon C and D (seabed) at the base and top, respectively. The composition of the SU-3 is similar to that of SU-2 (i.e. calcarenite and calcilutite on the shelf and chalk on the plateau), although cores from ODP 762 and 763 indicate calcareous oozes dominate around the Exmouth Plateau Arch. Biostratigraphic data (Fig. S1) show that Horizon C defines an unconformity between middle and late Miocene (~9 Ma), equivalent to Reflector 7 of Boyd *et al.* (1993) and N17-1 horizon of Hull and Griffiths (2002).

4.3.1 Basal surface: Horizon C

Horizon C is a low- to high-amplitude, relatively continuous reflection. In places, especially along the Kangaroo Syncline and on the flanks of the Exmouth Plateau Arch, it underlies chaotic seismic reflections (SF-4) (Figs 6a, d, and h).

4.3.2 Characteristics of SU-3

SU-3 is mainly contained in a depocentre in the NE-part of the study area, where it is up to 1000 m thick. The unit is thinnest (c. 50 m) across the Exmouth Plateau Arch (Fig. 7e). SU-3 contains two

451 dominant seismic facies (Fig. 7e): (i) SF-1, which is widespread across the study area (e.g. Figs 6c-d);
452 and (ii) SF-4, which dominates in the present-day bathymetric lows, such as along the Kangaroo
453 Syncline (Figs 6a, d, and h), and the western and southern flanks of the Exmouth Plateau Arch (Fig.
454 6g).

455 The 3D seismic reflection data partly imaged an area where SU-3 is dominated by stacked packages
456 of SF-4 (Fig. 11a). Locally, two horizons are mapped in the area (D-1-2), bounding at least three
457 packages of SF-4 (MTC-1-3) (Fig. 11a). Within these package we observe (Figs 11b-d): (i) 1-5 km wide
458 blocks of more coherent reflections and lateral margins (up to 200 m-deep) of MTC-1, between
459 Horizon C and D-1 (Figs 11a-b); (ii) up to 20 km-long erosional grooves that are best-expressed along
460 D-1 at the base of MTC-2 (Figs 11a and c); and (iii) primary and secondary flow fabrics (PFFs and
461 SFFs) with relief of ~30 m and lateral margin (~140 m-deep) of MTC-3 expressed on the seafloor (i.e.
462 Horizon D) (Figs 11a and d), from which MTC-3 can be divided into MTC-3 a and b. All of these
463 kinematic indicators are generally NW-trending, approximately the same with the trend of the
464 sediment wave crestlines within SU-2 (Figs 9b-d).

465 **4.3.3 Interpretation of SU-3**

466 SU-3 was deposited from ~9 Ma to the present. Biostratigraphic data indicate that, since the middle
467 Miocene, water depth in the Exmouth Plateau was generally bathyal (Fig. S4), with clinoforms height
468 in the Dampier Sub-basin suggesting water depths of at least 800 m based (Fig. 2) (Hull & Griffiths,
469 2002). Therefore, SU-3 deposition was significantly deeper than the previous SUs since the
470 beginning.

471 Thickness patterns of SU-3 suggest further growth of the Exmouth Plateau Arch during this time,
472 although a mismatch between the arch crest and the thinnest succession suggests that the uplift
473 occurred after the deposition of SU-3 (e.g. Fig. 6g). Coeval with the arch growth, deposition during
474 SU-3 times (Figs 6a, d, and 7e) was dominated by the emplacement of mass-transport complexes

(MTCs). Horizon C, which underlies these chaotic facies in many places, is therefore interpreted as a basal shear surface (BSS), along which materials were transported and deposited (Bull *et al.*, 2009). Elsewhere, pelagic and hemipelagic deposition occur (Fig. 7e).

Truncation of sub-parallel seismic reflections on the western flank of the Exmouth Plateau Arch (Fig. 6f-g) indicates that pelagic and hemipelagic deposits were modified by seabed erosion, most likely due to strong bottom current activity. Scarselli *et al.* (2013), who studied MTCs on the western flank of the Exmouth Plateau Arch (see Fig. 7e), document evidence for strong bottom currents along the headwall scarp of one of their MTCs. Further evidence for bottom current-driven erosion is documented on the eastern flank of the plateau, in the form of N-trending seabed furrows that cap underlying blocky MTCs (Day *et al.,* 2010). Similar interaction between MTCs and bottom currents, has also been documented elsewhere (e.g. Bahamas; e.g. Tournadour *et al.*, 2015; Wunsch *et al.*, 2017; South America; e.g. Krastel *et al.*, 2011). Despite the evidences of bottom current erosion, lack of bottom current depositional features on the plateau during SU-3 times most likely occurred because of the strong bottom current activity was coupled with the low sedimentation rate in this area (i.e. 20 m/Ma; Golovchenko *et al.*, 1992) compared to the shelf area (i.e. 175 - 275 m/Ma; Young *et al.*, 2001). Further landward of the plateau, the bottom current signal was masked by repetitive deposition of MTCs. These MTCs were predominantly deposited in present-day bathymetric lows (Fig. 7e) such as the Kangaroo Syncline (Figs 6a, d, and h). Based on the trend of headwall scarps on the seabed (Fig. 6e), and kinematic indicators beneath and within them (e.g. lateral margin and groove orientations, see Fig. 11), these stacked MTCs were derived from either the arch and transported landward, or from the shelf and transported seaward. The youngest shelf-derived MTCs (i.e. MTC-3 in Fig. 11a) have an estimated volume up to 100 km3 (Hengesh *et al.*, 2013), and can be classified as slope-attached MTCs (Moscardelli *et al.*, 2006; Moscardelli & Wood, 2016).

In terms of MTC genesis, this must be considered in light of the fact that slope failure occurs when the shear strength of a sediment (or material) is exceeded by the shear stress required for equilibrium (Hampton *et al.*, 1996; Duncan & Wright, 2005). Therefore, slope failure and MTC deposition can occur due to (i) shear stress increases (e.g. due to an earthquake-related seismic shaking), (ii) slope oversteepening (e.g. related to increased sediment influx or to tectonics), and/or (iii) shear strength decreases (e.g. due to fluid expulsion, gas hydrate dissociation, and/or high sedimentation rates) (e.g. Hampton *et al.*, 1996; Locat & Lee, 2002). Bottom simulating reflectors (BSRs), indicative of gas hydrates (e.g. Hyndman & Spence, 1992), are absent within the study area (Scarselli *et al.*, 2013). Furthermore, Neogene sedimentation rates on the Exmouth Plateau are relatively low (20 m/Ma) (Golovchenko *et al.*, 1992). This is 40 times lower than many basins that become overpressured due to high sediment accumulation rates, such as in Tertiary delta provinces (e.g. Osborne & Swarbrick, 1997). Gas hydrate dissociation and high sedimentation rates are therefore not considered as triggering mechanisms for MTCs emplacement in the study area, although the VFZ might indicate gas hydrate dissociation during SU-2 times. In contrast, seismic shaking due to earthquakes, tectonically-related slope oversteepening, and fluid expulsion might be considered potential triggers for slope failure and MTC emplacement on the Exmouth Plateau. Tectonic reactivation of pre-existing structures along the NW Shelf of Australia, possibly related to plate collision along the northern margin, could have induced slope oversteepening in concert with increased seismicity (Keep *et al.*, 1998). Tectonically-related arching of the NE-trending Exmouth Plateau Arch probably led to the deposition of MTCs from the arch crest to the east (landward) and west (seaward) (Boyd *et al.*, 1993; Hengesh *et al.*, 2013; Scarselli *et al.*, 2013). Subsurface fluid migration and trapping in impermeable layers may have also ‘primed’ the slope to fail, although seabed pockmarks provide some evidence for fluid venting (Hengesh *et al.*, 2013).

5. Discussion

We have shown that the Late Cretaceous to late Miocene deposition on the Exmouth Plateau was dominated by slope-parallel bottom currents (producing both depositional and erosional features), whereas post-Miocene deposition was dominated by down-slope, gravity-driven processes (mainly manifested as MTCs). In this section, we discuss the significance of this change in dominant process regime, in particular how this may correlate with sediment supply, regional tectonics and palaeo-oceanographic events that were occurring simultaneously along the southern and northern margins of Australia. In addition, we will discuss how local structural complexities on the Exmouth Plateau influence depositional processes.

5.1 Palaeo-oceanographic evolution of the NW Australia continental margin

Our results show that the Late Cretaceous to Present succession offshore NW Australia archives two major events that impacted global thermohaline ocean circulation, with the Exmouth Plateau uniquely located between oceanic gateways that were either opening (i.e. Tasman Gap) or closing (i.e. Indonesian Seaway) during deposition (Knutz, 2008). A period of major tectonic plate reorganisation occurred in the Late Cretaceous (Cenomanian, ~100 Ma) (Powell *et al.*, 1988; Veevers *et al.*, 1991). Oceanic crust was generated as a result of seafloor spreading between Australia and Antarctica (Figs 2 and 12a) (Baillie *et al.*, 1994), with the deep-ocean connecting western Australia to the Pacific Ocean forming in the Oligocene. This implies that the circum-polar current around Antarctica was deflected onto the western margin of Australia from the Cretaceous until the late Palaeogene (Baillie *et al.*, 1994). The widespread base Turonian (~93.9 Ma) erosional surface (i.e. Horizon A), and subsequent SU-1 contourite channels and furrows (Fig. 12a), on the Exmouth Plateau may record initiation of this circum-polar current, herein interpreted as the palaeo-WAC. Our interpretation of this bottom current direction, i.e. NE-flowing, is consistent with global reconstruction of Late Cretaceous oceans using numerical modelling and biostratigraphy (Fig. 12a)

(Poulsen *et al.*, 2001; Pucéat *et al.*, 2005). Global reconstruction of the ocean currents also agrees with contourite deposition on the plateau before the Turonian, i.e. Albian (Romine *et al.*, 1997; Young *et al.*, 2001), manifested as the pre-SU-1 mounds (see Fig. 7b).

After a ~27 Myr period of bottom current activity and contourite deposition, another major erosional event occurred at the end Cretaceous (~66 Ma) (Horizon B). This event coincides with the change of the primary ocean spreading axis from the Indian Ocean to the Southern Ocean (Powell *et al.*, 1988) (Fig. 12b), which marked initial opening of the major ocean gateway between Australia and Antarctica, i.e. Tasman Gap (Fig. 12b). The Tasman Gap opened rapidly from the late Eocene to early Oligocene (Stickley *et al.*, 2004; Houben *et al.*, 2013). In contrast, timing of the opening of Drake Passage, an ocean gateway between South America and Antarctica, is less well constrained, but is thought to begin in the middle Eocene (e.g. Scher & Martin, 2006; Livermore *et al.*, 2007), eventually taking its modern form by the Miocene (Beu *et al.*, 1997; Kuhnert *et al.*, 2009). As both ocean gateways open, circum-polar ocean current circulation around Antarctica became fully established (Miller *et al.*, 1991). The establishment of circum-polar circulation, and genetically-related continental ice sheet build-up on Antarctica, led to a global sea level fall (Miller *et al.*, 1991). We suggest that a deepening of bottom current activity due to a eustatic sea-level fall, combined with a strengthening of the associated palaeo-WAC, is recorded on the Exmouth Plateau by the growth of sediment waves, and the development of NE-trending deep scours, especially in the transition zone into the VFZ (Figs 9 and 12b). We infer the flow direction of bottom currents responsible for the development of these features is similar to that of SU-1, i.e. to the NE. This interpretation is consistent with the prediction of numerical models, that show NE-flowing currents along the Cenozoic NW shelf of Australia (see Fig. 12b) (Barrow and Peterson, 1991). The Leeuwin Current (LC), although has potentially been active during SU-2 times (see Fig. 2), is unlikely to be responsible for the formation of erosional and depositional features preserved in SU-2 because of its

571 shallow depth of operation (<300 m). This interpretation is supported by the Quaternary record,
572 with the WAC being stronger than the LC during glacial periods (Spooner *et al.*, 2011).

573 During SU-3 deposition, bottom current activity might have been masked by down-slope
574 depositional processes dominated by deposition of MTCs. We attribute this change in depositional
575 style to reflect increased tectonic activity along the northern margin of Australia, related to the
576 collision between the northward-moving Australian Plate, and the Pacific and Eurasia plates, which
577 began in the early Miocene (Boyd *et al.*, 1993; Baillie *et al.*, 1994). Coeval with this collision was a
578 change in climate in NW Australia, from humid (at 5.5 Ma) to arid (at 2.4 Ma), as a result of the
579 progressive constriction of the Indonesian Throughflow along the northern margin of Australia (see
580 Figs 1a and 2) (Christensen *et al.*, 2017). Moreover, tectonic activity also coincided with a dramatic
581 increase (from c. 1000 to c. 5000 km^3/Ma) in sedimentation rates on the adjacent shelf and slope
582 from SU-2 to SU-3 times (Young *et al.*, 2001). Although MTCs are ubiquitous, bottom current-related
583 deposits are still observed, for example, in late middle Miocene, NE-prograding contourite preserved
584 in the Dampier Sub-basin (Cathro *et al.*, 2003) (see also Day *et al.*, 2010 and Scarselli *et al.*, 2013).
585 This implies that the WAC rather than the Leeuwin Current is still influencing the seabed of the >800
586 m deep plateau, the latter only operating down to relatively shallow (<300 m) water depths (Fig. 3).

587 Few studies have used seismic reflection data to document pre-Quaternary bottom current activity
588 and related deposits (Romine *et al.*, 1997; Young *et al.*, 2001; Cathro *et al.*, 2003). Our
589 documentation of widespread evidence for erosional and depositional, bottom current-related
590 features on the plateau advance our understanding of the palaeo-oceanographic evolution of
591 offshore Western Australia. Previous studies have been conducted using various proxies, such as
592 Mg/Ca ratio, carbon and oxygen isotopes, and foraminifera assemblages (Wells & Wells, 1994; Sinha
593 *et al.*, 2006; Murgese & De Deckker, 2007; Karas *et al.*, 2011; Spooner *et al.*, 2011), but have only
594 extended palaeo-oceanographic history to the early Pleistocene (2.2 Ma) (Sinha *et al.*, 2006).

5.2 Influence of local structural features on depositional processes

Depositional processes on the Exmouth Plateau was not only influenced by regional events occurring along the southern and northern margins of Australia, but also the development of more local structural features. During SU-1 times, the Resolution Arch, which defines the eastern margin of the plateau, was growing (see Fig. 7a) (Young *et al.*, 2001); the western margin of the plateau still represent a bathymetric high after breakup (see Fig. 6f) (Boyd *et al.*, 1993). These two features served to focus bottom current pathways, which then controlled the locations of the pre-SU-1 mounds and SU-1 contourite channels (see Fig 7b-c). Internally, substantial relief across the pre-SU-1 mounds (c. 500 m) also controlled subsequent erosional and depositional processes (see Fig. 6a). SU-2 deposition was coeval with the growth of the Exmouth Plateau Arch (Boyd *et al.*, 1993), thus bottom currents pathways were more focused between the arch and eastern margin of the plateau (see Fig. 7d). In addition, relief across the pre-SU-1 mounds also controlled the geometry and location of SU-2 contourite channels, which were deflected along the mound flanks (Fig. 6c and Fig. 7d). In contrast, the western margin of the plateau (seaward from the western flank of the Exmouth Plateau Arch) has progressively subsided and was less influenced by bottom currents, most likely because of less bathymetric constriction as it has been exposed to open ocean. During SU-3 times, although MTCs deposition dominated, bottom currents features such as the N-trending furrows of Day *et al.* (2010) and erosion along MTCs headscarp of Scarselli *et al.* (2013) provide evidences of how local bathymetric variation controls bottom currents pathway. Therefore, examples from each SU prove that bathymetric framework dictates contourites depositional and erosional processes (e.g. Faugères & Stow, 2008; Pérez *et al.*, 2014).

6. Conclusions

The Late Cretaceous to present-day history of the Exmouth Plateau (offshore NW Australia) records a prolonged period of deep-marine, fine-grained, carbonate-dominated sedimentation, comprising the variable interaction of oceanic bottom currents, large-scale gravity flows and hemipelagic

processes. The geological history is captured in three regionally-extensive tectono-stratigraphic units (SU1-3), which have been defined from an integrate analysis of 2D and 3D seismic reflection and borehole data.

The Late Cretaceous interval (SU-1) is dominated by a range of seismic-scale constructional bedforms (e.g. contourite drift) and erosional features (e.g. contourite channel), which formed in palaeo-water depths of c. 200 m in response to strong oceanic bottom-currents. These currents are inferred to have been the ancient precursors of the major oceanic circulation systems of the present-day Indian and Southern oceans. During this time, the circum-polar ocean current, which circulates around the Antarctica in the present-day Southern Ocean, was deflected along the western margin of Australia. Hence, this circum-polar ocean current is interpreted as the palaeo-West Australian Current (WAC).

The Palaeocene to late Miocene interval (SU-2) is characterised by: (i) very large (amplitude, c. 40 m and wavelength, c. 3 km), SW-migrating, NW-SE-trending sediment waves, (ii) large (4 km-wide, 100 m-deep), NE-trending scours that flank the sediment waves, and (iii) NW-trending, 4 km wide and 80 m deep turbidite channel, infilled by NE-dipping reflectors, which formed in water depths of c. 200-600 m due to ongoing bottom current activity. These features were formed by NE-flowing bottom currents (palaeo-WAC), which are thought to have intensified during a glacial period following the establishment of circum-polar ocean circulation around Antarctica.

The late Miocene to present-day interval (SU-3) comprises large (up to 100 km^3), widespread mass-transport complexes (MTCs), which accumulated in palaeo-water depths of c. 800 m. Bottom-current activity in the form of furrows and other erosional features along seafloor scarps was relatively minor. The MTCs were derived from two sediment sources: (i) the continental margin to the SE, and (ii) the Exmouth Plateau Arch to the NW. The MTCs were probably triggered by a combination of (i) tectonically-induced oversteepening of the continental margin, and (ii) regional

644 folding of the intra-basin Exmouth Plateau Arch. These processes can be linked to ongoing collision
645 along the northern margin of the Australia plate.

646 Hence, the tectono-stratigraphic and palaeo-oceanographic evolution of the Exmouth Plateau is
647 related to two regional geological events: (i) earlier rifting and the opening of an ocean gateway
648 along the southern margin of the continent, and (ii) later collision and associated closure of an ocean
649 gateway along the northern margin of the continent.

650 **7. Acknowledgements**

651 We thank Geoscience Australia for providing seismic and borehole data, IODP for providing ODP wells,
652 and Schlumberger for providing software. The first author thanks the Indonesia Endowment Fund for
653 Education (LPDP) (Grant No.: 20160822019161) for its financial support. We thank the editor, Atle
654 Rotevatn, for his supportive and constructive comments, and the reviewers, Lara F. Pérez and Zane
655 Jobe, for thorough, constructive reviews to improve an earlier version of this manuscript.

656 **8. Conflict of Interest**

657 No conflict of interest declared.

658 **9. References**

659 AKHURST, M.C., STOW, D.A. & STOKER, M.S. (2002) Late Quaternary Glacigenic Contourite, Debris Flow
660 and Turbidite Process Interaction in the Faroe-Shetland Channel, Nw European Continental
661 Margin. *Geological Society, London, Memoirs*, **22,** 73-84.
662 ALFARO, E. & HOLZ, M. (2014) Seismic Geomorphological Analysis of Deepwater Gravity-Driven
663 Deposits on a Slope System of the Southern Colombian Caribbean Margin. *Marine and*
664 *Petroleum Geology*, **57,** 294-311.
665 ARMANDITA, C., MORLEY, C.K. & ROWELL, P. (2015) Origin, Structural Geometry, and Development of a
666 Giant Coherent Slide: The South Makassar Strait Mass Transport Complex. *Geosphere*, **11,**
667 376-403.

668 BAGGULEY, J. & PROSSER, S. (1999) The Interpretation of Passive Margin Depositional Processes Using
669 Seismic Stratigraphy: Examples from Offshore Namibia. *Geological Society, London, Special*
670 *Publications*, **153,** 321-344.
671 BAILLIE, P., POWELL, C.M., LI, Z. & RYALL, A. (1994). *The Tectonic Framework of Western Australia's*
672 *Neoproterozoic to Recent Sedimentary Basins*. The Sedimentary Basins of Western Australia:
673 Proceedings of Petroleum Exploration Society of Australia Symposium.
674 BARRON, E.J. & PETERSON, W.H. (1991) The Cenozoic Ocean Circulation Based on Ocean General
675 Circulation Model Results. *Palaeogeography, Palaeoclimatology, Palaeoecology*, **83,** 1-28.
676 BEU, A., GRIFFIN, M. & MAXWELL, P. (1997) Opening of Drake Passage Gateway and Late Miocene to
677 Pleistocene Cooling Reflected in Southern Ocean Molluscan Dispersal: Evidence from New
678 Zealand and Argentina. *Tectonophysics*, **281,** 83-97.
679 BLUMSACK, S. & WEATHERLY, G. (1989) Observations of the Nearby Flow and a Model for the Growth of
680 Mudwaves. *Deep Sea Research Part A. Oceanographic Research Papers*, **36,** 1327-1339.
681 BOYD, R., WILLIAMSON, P. & HAQ, B. (1993) Seismic Stratigraphy and Passive-Margin Evolution of the
682 Southern Exmouth Plateau. In: *Sequence Stratigraphy and Facies Associations* (Ed. by H. W.
683 Posamentier, C. P. Summerhayes, B. U. Haq & G. P. Allen), **18**, 579-603. Blackwell Scientific
684 Publications, Oxford.
685 BROWN, A.R. (2011) *Interpretation of Three-Dimensional Seismic Data*. The American Association of
686 Petroleum Geologists and the Society of Exploration Geophysicists, Tulsa.
687 BULL, S., CARTWRIGHT, J. & HUUSE, M. (2009) A Review of Kinematic Indicators from Mass-Transport
688 Complexes Using 3d Seismic Data. *Marine and Petroleum Geology*, **26,** 1132-1151.
689 CATHRO, D.L., AUSTIN JR, J.A. & MOSS, G.D. (2003) Progradation Along a Deeply Submerged
690 Oligocenemiocene Heterozoan Carbonate Shelf: How Sensitive Are Clinoforms to Sea Level
691 Variations? *AAPG bulletin*, **87,** 1547-1574.

692 CATHRO, D.L. & KARNER, G.D. (2006) Cretaceous–Tertiary Inversion History of the Dampier Sub-Basin,
693 Northwest Australia: Insights from Quantitative Basin Modelling. *Marine and Petroleum*
694 *Geology*, **23,** 503-526.
695 CHRISTENSEN, B.A., RENEMA, W., HENDERIKS, J., DE VLEESCHOUWER, D., GROENEVELD, J., CASTAÑEDA, I.S.,
696 REUNING, L., BOGUS, K., AUER, G. & ISHIWA, T. (2017) Indonesian Throughflow Drove Australian
697 Climate from Humid Pliocene to Arid Pleistocene. *Geophysical Research Letters*, **44,** 6914-
698 6925.
699 CLARK, I., CARTWRIGHT, J., PRATHER, B., DEPTUCK, M., MOHRIG, D., VAN HOORN, B. & WYNN, R. (2012)
700 Interactions between Coeval Sedimentation and Deformation from the Niger Delta
701 Deepwater Fold Belt. In: *Application of the Principles Seismic Geomorphology to Continental*
702 *Slope and Base-of-Slope Systems: Case Studies from Seafloor and near-Seafloor Analogues*
703 (Ed. by B. Prather, M. E. Deptuck, D. Mohrig, B. V. Hoorn & R. Wynn), *Sepm Special*
704 *Publication*, **99**, 243-267. SEPM (Society for Sedimentary Geology).
705 COLLINS, L.B., JAMES, N.P. & BONE, Y. (2014) Carbonate Shelf Sediments of the Western Continental
706 Margin of Australia. *Geological Society, London, Memoirs*, **41,** 255-272.
707 COVAULT, J.A., ROMANS, B.W., GRAHAM, S.A., FILDANI, A. & HILLEY, G.E. (2011) Terrestrial Source to Deep-
708 Sea Sink Sediment Budgets at High and Low Sea Levels: Insights from Tectonically Active
709 Southern California. *Geology*, **39,** 619-622.
710 DAVIES, T. & LAUGHTON, A. (1972) Sedimentary Processes in the North Atlantic. *Initial reports of the*
711 *deep sea drilling project*, **12,** 905-934.
712 DAY, K., GALE, J. & SMALLWOOD, J. (2010) Deepwater Exmouth Plateau, North Carnarvon Basin:
713 Preliminary Investigations into Ridge and Furrow Features. *APPEA*, **50,** 731-731.
714 DUNCAN, J. & WRIGHT, S. (2005) Soil Strength and Slope Stability, John Wiley & Sons Ltd.
715 ERCILLA, G., JUAN, C., HERNANDEZ-MOLINA, F.J., BRUNO, M., ESTRADA, F., ALONSO, B., CASAS, D., LÍ FARRAN, M.,
716 LLAVE, E. & GARCIA, M. (2016) Significance of Bottom Currents in Deep-Sea Morphodynamics:
717 An Example from the Alboran Sea. *Marine Geology*, **378,** 157-170.

718 ESMERODE, E.V., LYKKE-ANDERSEN, H. & SURLYK, F. (2008) Interaction between Bottom Currents and
719 Slope Failure in the Late Cretaceous of the Southern Danish Central Graben, North Sea.
720 *Journal of the Geological Society*, **165,** 55-72.
721 EXON, N., HAQ, B. & VON RAD, U. (1992) Exmouth Plateau Revisited: Scientific Drilling and Geological
722 Framework. In: *Proceedings of the Ocean Drilling Program, Scientific Results* (Ed. by U. Von
723 Rad, B. U. Haq, R. B. Kidd & S. B. O'Connell), **122**, 3-20. Ocean Drilling Program, College
724 Station, TX.
725 EXON, N.F. & WILLCOX, J.B. (1980) *The Exmouth Plateau: Stratigraphy, Structure, and Petroleum*
726 *Potential*. Australian Government Publishing Service, Canberra.
727 FALVEY, D. & VEEVERS, J. (1974) Physiography of the Exmouth and Scott Plateaus, Western Australia,
728 and Adjacent Northeast Wharton Basin. *Marine Geology*, **17,** 21-59.
729 FAUGÈRES, J.-C. & STOW, D.A. (1993) Bottom-Current-Controlled Sedimentation: A Synthesis of the
730 Contourite Problem. *Sedimentary Geology*, **82,** 287-297.
731 FAUGÈRES, J.-C., STOW, D.A., IMBERT, P. & VIANA, A. (1999) Seismic Features Diagnostic of Contourite
732 Drifts. *Marine Geology*, **162,** 1-38.
733 FAUGÈRES, J.-C. & STOW, D. (2008) Contourite Drifts: Nature, Evolution and Controls. *Developments in*
734 *sedimentology*, **60,** 257-288.
735 FLOOD, R.D. (1988) A Lee Wave Model for Deep-Sea Mudwave Activity. *Deep Sea Research Part A.*
736 *Oceanographic Research Papers*, **35,** 973-983.
737 GAMBOA, D., ALVES, T., CARTWRIGHT, J. & TERRINHA, P. (2010) Mtd Distribution on a 'Passive' Continental
738 Margin: The Espírito Santo Basin (Se Brazil) During the Palaeogene. *Marine and Petroleum*
739 *Geology*, **27,** 1311-1324.
740 GARCÍA, M., ERCILLA, G. & ALONSO, B. (2009a) Morphology and Sedimentary Systems in the Central
741 Bransfield Basin, Antarctic Peninsula: Sedimentary Dynamics from Shelf to Basin. *Basin*
742 *Research*, **21,** 295-314.

743 GARCÍA, M., HERNÁNDEZ-MOLINA, F., LLAVE, E., STOW, D., LEÓN, R., FERNÁNDEZ-PUGA, M., DEL RÍO, V.D. &
744 SOMOZA, L. (2009b) Contourite Erosive Features Caused by the Mediterranean Outflow Water
745 in the Gulf of Cadiz: Quaternary Tectonic and Oceanographic Implications. *Marine Geology*,
746 **257,** 24-40.
747 GEE, M., GAWTHORPE, R. & FRIEDMANN, S. (2006) Triggering and Evolution of a Giant Submarine
748 Landslide, Offshore Angola, Revealed by 3d Seismic Stratigraphy and Geomorphology.
749 *Journal of Sedimentary Research*, **76,** 9-19.
750 GEE, M., UY, H., WARREN, J., MORLEY, C. & LAMBIASE, J. (2007) The Brunei Slide: A Giant Submarine
751 Landslide on the North West Borneo Margin Revealed by 3d Seismic Data. *Marine Geology*,
752 **246,** 9-23.
753 GOLOVCHENKO, X., BORELLA, P.E. & O'CONNELL, S.B. (1992) Sedimentary Cycles on the Exmouth Plateau.
754 In: *Proceedings of the Ocean Drilling Program, Scientific Results* (Ed. by U. Von Rad, B. U.
755 Haq, R. B. Kidd & S. B. O'Connell), **122**, 279-291. Ocean Drilling Program, College Station, TX.
756 GRADSTEIN, F.M., OGG, J.G., SCHMITZ, M. & OGG, G. (2012) *The Geologic Time Scale 2012*. Elsevier.
757 GRUETZNER, J. & UENZELMANN-NEBEN, G. (2016) Contourite Drifts as Indicators of Cenozoic Bottom
758 Water Intensity in the Eastern Agulhas Ridge Area, South Atlantic. *Marine Geology*, **378,** 350-
759 360.
760 HAMPTON, M.A., LEE, H.J. & LOCAT, J. (1996) Submarine Landslides. *Reviews of Geophysics*, **34,** 33-59.
761 HAQ, B.U., HARDENBOL, J. & VAIL, P.R. (1987) Chronology of Fluctuating Sea Levels since the Triassic.
762 *Science*, **235,** 1156-1167.
763 HAQ, B.U., BOYD, R.L., EXON, N.F. & VON RAD, U. (1992) Evolution of the Central Exmouth Plateau: A
764 Post-Drilling Perspective. In: *Proceedings of the Ocean Drilling Program, Scientific Results*
765 (Ed. by U. Von Rad, B. U. Haq, R. B. Kidd & S. B. O'Connell), **122**, 801-816. Ocean Drilling
766 Program, College Station, TX.
767 HEINIO, P. & DAVIES, R. (2006) Degradation of Compressional Fold Belts: Deep-Water Niger Delta.
768 *AAPG Bulletin*, **90,** 753-770.

769 HENGESH, J.V., DIRSTEIN, J.K. & STANLEY, A.J. (2013) Landslide Geomorphology Along the Exmouth
770 Plateau Continental Margin, North West Shelf, Australia. *Australian Geomechanics*, **48,** 71-
771 92.
772 HERNÁNDEZ-MOLINA, F., LARTER, R., REBESCO, M. & MALDONADO, A. (2006a) Miocene Reversal of Bottom
773 Water Flow Along the Pacific Margin of the Antarctic Peninsula: Stratigraphic Evidence from
774 a Contourite Sedimentary Tail. *Marine Geology*, **228,** 93-116.
775 HERNÁNDEZ-MOLINA, F., LLAVE, E. & STOW, D. (2008) Continental Slope Contourites. *Developments in*
776 *Sedimentology*, **60,** 379-408.
777 HERNÁNDEZ-MOLINA, F.J., LLAVE, E., STOW, D., GARCÍA, M., SOMOZA, L., VÁZQUEZ, J.T., LOBO, F., MAESTRO, A.,
778 DEL RÍO, V.D. & LEÓN, R. (2006b) The Contourite Depositional System of the Gulf of Cadiz: A
779 Sedimentary Model Related to the Bottom Current Activity of the Mediterranean Outflow
780 Water and Its Interaction with the Continental Margin. *Deep Sea Research Part II: Topical*
781 *Studies in Oceanography*, **53,** 1420-1463.
782 HERNÁNDEZ-MOLINA, F.J., SOTO, M., PIOLA, A.R., TOMASINI, J., PREU, B., THOMPSON, P., BADALINI, G., CREASER,
783 A., VIOLANTE, R.A. & MORALES, E. (2016) A Contourite Depositional System Along the
784 Uruguayan Continental Margin: Sedimentary, Oceanographic and Paleoceanographic
785 Implications. *Marine Geology*, **378,** 333-349.
786 HOFSTRA, M., PEAKALL, J., HODGSON, D. & STEVENSON, C. (2018) Architecture and Morphodynamics of
787 Subcritical Sediment Waves in an Ancient Channel–Lobe Transition Zone. *Sedimentology***,**
788 doi:10.1111/sed.12468
789 HOUBEN, A.J., BIJL, P.K., PROSS, J., BOHATY, S.M., PASSCHIER, S., STICKLEY, C.E., RÖHL, U., SUGISAKI, S., TAUXE, L.
790 & VAN DE FLIERDT, T. (2013) Reorganization of Southern Ocean Plankton Ecosystem at the
791 Onset of Antarctic Glaciation. *Science*, **340,** 341-344.
792 HULL, J.N.F. & GRIFFITHS, C.M. (2002). *Sequence Stratigraphic Evolution of the Albian to Recent Section*
793 *of the Dampier Sub-Basin, Northwest Shelf, Australia*. The Sedimentary Basins of Western
794 Australia 3: Proceedings of the Petroleum Exploration Society of Australia Symposium, Perth.

795 HUNEKE, H. & MULDER, T. (2010) *Deep-Sea Sediments*. Elsevier.
796 HYNDMAN, R. & SPENCE, G. (1992) A Seismic Study of Methane Hydrate Marine Bottom Simulating
797 Reflectors. *Journal of Geophysical Research: Solid Earth*, **97,** 6683-6698.
798 IMBERT, P. & HO, S. (2012) Seismic-Scale Funnel-Shaped Collapse Features from the Paleocene–
799 Eocene of the North West Shelf of Australia. *Marine Geology*, **332,** 198-221.
800 JAMES, N.P., BONE, Y., KYSER, T.K., DIX, G.R. & COLLINS, L.B. (2004) The Importance of Changing
801 Oceanography in Controlling Late Quaternary Carbonate Sedimentation on a High-Energy,
802 Tropical, Oceanic Ramp: North-Western Australia. *Sedimentology*, **51,** 1179-1205.
803 JOHNSON, D.A. & DAMUTH, J.E. (1979) Deep Thermohaline Flow and Current-Controlled Sedimentation
804 in the Amirante Passage: Western Indian Ocean. *Marine Geology*, **33,** 1-44.
805 KÄHLER, G. & STOW, D.A. (1998) Turbidites and Contourites of the Palaeogene Lefkara Formation,
806 Southern Cyprus. *Sedimentary Geology*, **115,** 215-231.
807 KARAS, C., NÜRNBERG, D., TIEDEMANN, R. & GARBE-SCHÖNBERG, D. (2011) Pliocene Indonesian
808 Throughflow and Leeuwin Current Dynamics: Implications for Indian Ocean Polar Heat Flux.
809 *Paleoceanography*, **26,** PA2217.
810 KARNER, G.D. & DRISCOLL, N.W. (1999) Style, Timing and Distribution of Tectonic Deformation across
811 the Exmouth Plateau, Northwest Australia, Determined from Stratal Architecture and
812 Quantitative Basin Modelling. *Geological Society, London, Special Publications*, **164,** 271-311.
813 KEEP, M., POWELL, C. & BAILLIE, P. (1998) Neogene Deformation of the North West Shelf, Australia. *The*
814 *sedimentary basins of Western Australia*, **2,** 81-91.
815 KEEP, M., HARROWFIELD, M. & CROWE, W. (2007) The Neogene Tectonic History of the North West Shelf,
816 Australia. *Exploration Geophysics*, **38,** 151-174.
817 KELMAN, A.P., NICOLL, R.S., KENNARD, J.M., MORY, A.J., MANTLE, D.J., POIDEVIN, S.L., BERNARDEL, G., ROLLET,
818 N. & EDWARDS, D. (2013) Northern Carnarvon Basin Biozonation and Stratigraphy, Chart 36,
819 Geoscience Australia.

KNUTZ, P. (2008) Palaeoceanographic Significance of Contourite Drifts. *Developments in Sedimentology*, **60,** 511-535.

KRASTEL, S., WEFER, G., HANEBUTH, T.J., ANTOBREH, A.A., FREUDENTHAL, T., PREU, B., SCHWENK, T., STRASSER, M., VIOLANTE, R. & WINKELMANN, D. (2011) Sediment Dynamics and Geohazards Off Uruguay and the De La Plata River Region (Northern Argentina and Uruguay). *Geo-Marine Letters*, **31,** 271-283.

KUHNERT, H., BICKERT, T. & PAULSEN, H. (2009) Southern Ocean Frontal System Changes Precede Antarctic Ice Sheet Growth During the Middle Miocene. *Earth and Planetary Science Letters*, **284,** 630-638.

LIVERMORE, R., HILLENBRAND, C.D., MEREDITH, M. & EAGLES, G. (2007) Drake Passage and Cenozoic Climate: An Open and Shut Case? *Geochemistry, Geophysics, Geosystems*, **8**.

LLAVE, E., JANÉ, G., MAESTRO, A., LÓPEZ-MARTÍNEZ, J., HERNÁNDEZ-MOLINA, F.J. & MINK, S. (2018) Geomorphological and Sedimentary Processes of the Glacially Influenced Northwestern Iberian Continental Margin and Abyssal Plains. *Geomorphology*, **312,** 60-85.

LOCAT, J. & LEE, H.J. (2002) Submarine Landslides: Advances and Challenges. *Canadian Geotechnical Journal*, **39,** 193-212.

LONERGAN, L., JAMIN, N.H., JACKSON, C.A.-L. & JOHNSON, H.D. (2013) U-Shaped Slope Gully Systems and Sediment Waves on the Passive Margin of Gabon (West Africa). *Marine Geology*, **337,** 80-97.

LONGLEY, I.M., BUESSENSCHUETT, C., CLYDSDALE, L., CUBITT, C.J., DAVIS, R.C., JOHNSON, M.K., MARSHALL, N.M., MURRAY, A.P., SOMERVILLE, R. & SPRY, T.B. (2002) The North West Shelf of Australia - a Woodside Perspective. *The Sedimentary Basins of Western Australia 3: Petroleum Exploration Society of Australia Symposium*. M. Keep & S. J. Moss. Perth**,** 28-88.

MARCHÈS, E., MULDER, T., GONTHIER, E., CREMER, M., HANQUIEZ, V., GARLAN, T. & LECROART, P. (2010) Perched Lobe Formation in the Gulf of Cadiz: Interactions between Gravity Processes and Contour Currents (Algarve Margin, Southern Portugal). *Sedimentary Geology*, **229,** 81-94.

MARTORELLI, E., BOSMAN, A., CASALBORE, D. & FALCINI, F. (2016) Interaction of Down-Slope and Along-Slope Processes Off Capo Vaticano (Southern Tyrrhenian Sea, Italy), with Particular Reference to Contourite-Related Landslides. *Marine Geology*, **378,** 43-55.

MARTOS, Y.M., MALDONADO, A., LOBO, F.J., HERNÁNDEZ-MOLINA, F.J. & PÉREZ, L.F. (2013) Tectonics and Palaeoceanographic Evolution Recorded by Contourite Features in Southern Drake Passage (Antarctica). *Marine Geology*, **343,** 76-91.

MASSON, D., WYNN, R. & TALLING, P. (2010) Large Landslides on Passive Continental Margins: Processes, Hypotheses and Outstanding Questions. In: *Submarine Mass Movements and Their Consequences* (Ed. by D. C. Mosher, C. Shipp, L. Moscardelli, J. D. Chaytor, C. D. P. Baxter, H. J. Lee & R. Urgeles), 153-165. Springer, Dordrecht.

MCGOWRAN, B., LI, Q., CANN, J., PADLEY, D., MCKIRDY, D.M. & SHAFIK, S. (1997) Biogeographic Impact of the Leeuwin Current in Southern Australia since the Late Middle Eocene. *Palaeogeography, Palaeoclimatology, Palaeoecology*, **136,** 19-40.

MICHELS, K.H., ROGENHAGEN, J. & KUHN, G. (2001) Recognition of Contour-Current Influence in Mixed Contourite-Turbidite Sequences of the Western Weddell Sea, Antarctica. *Marine Geophysical Researches*, **22,** 465-485.

MILLER, K.G., WRIGHT, J.D. & FAIRBANKS, R.G. (1991) Unlocking the Ice House: Oligocene-Miocene Oxygen Isotopes, Eustasy, and Margin Erosion. *Journal of Geophysical Research: Solid Earth*, **96,** 6829-6848.

MOSCARDELLI, L., WOOD, L. & MANN, P. (2006) Mass-Transport Complexes and Associated Processes in the Offshore Area of Trinidad and Venezuela. *AAPG Bulletin*, **90,** 1059-1088.

MOSCARDELLI, L. & WOOD, L. (2016) Morphometry of Mass-Transport Deposits as a Predictive Tool. *GSA Bulletin*, **128,** 47-80.

MULDER, T., LECROART, T., VOISSET, M., SCHÖNFELD, J., LE DREZEN, E., GONTHIER, E., HANQUIEZ, V., ZAHN, R., FAUGÈRES, J.C. & HERNANDEZ-MOLINA, F. (2002) Past Deep-Ocean Circulation and the

Paleoclimate Record-Gulf of Cadiz. *EOS, Transactions American Geophysical Union*, **83,** 481-488.

MULDER, T., LECROART, P., HANQUIEZ, V., MARCHES, E., GONTHIER, E., GUEDES, J.-C., THIÉBOT, E., JAAIDI, B., KENYON, N. & VOISSET, M. (2006) The Western Part of the Gulf of Cadiz: Contour Currents and Turbidity Currents Interactions. *Geo-Marine Letters*, **26,** 31-41.

MÜLLER, R., DYKSTERHUIS, S. & REY, P. (2012) Australian Paleo-Stress Fields and Tectonic Reactivation over the Past 100 Ma. *Australian Journal of Earth Sciences*, **59,** 13-28.

MÜLLER, R., DUTKIEWICZ, A., SETON, M. & GAINA, C. (2013) Seawater Chemistry Driven by Supercontinent Assembly, Breakup, and Dispersal. *Geology*, **41,** 907-910.

MURGESE, D.S. & DE DECKKER, P. (2007) The Late Quaternary Evolution of Water Masses in the Eastern Indian Ocean between Australia and Indonesia, Based on Benthic Foraminifera Faunal and Carbon Isotopes Analyses. *Palaeogeography, Palaeoclimatology, Palaeoecology*, **247,** 382-401.

NORMARK, W.R., PIPER, D.J. & SLITER, R. (2006) Sea-Level and Tectonic Control of Middle to Late Pleistocene Turbidite Systems in Santa Monica Basin, Offshore California. *Sedimentology*, **53,** 867-897.

ORTIZ-KARPF, A., HODGSON, D.M., JACKSON, C.A.L. & MCCAFFREY, W.D. (2016) Mass-Transport Complexes as Markers of Deep-Water Fold-and-Thrust Belt Evolution: Insights from the Southern Magdalena Fan, Offshore Colombia. *Basin Research*, **30,** 65-88.

OSBORNE, M.J. & SWARBRICK, R.E. (1997) Mechanisms for Generating Overpressure in Sedimentary Basins: A Reevaluation. *AAPG bulletin*, **81,** 1023-1041.

PEARCE, A. (1991) Eastern Boundary Currents of the Southern Hemisphere. *Journal of the Royal Society of Western Australia*, **74,** 35-45.

PÉREZ, L.F., MALDONADO, A., BOHOYO, F., HERNÁNDEZ-MOLINA, F.J., VÁZQUEZ, J.T., LOBO, F.J. & MARTOS, Y.M. (2014) Depositional Processes and Growth Patterns of Isolated Oceanic Basins: The

Protector and Pirie Basins of the Southern Scotia Sea (Antarctica). *Marine Geology*, **357,** 163-181.

PÉREZ, L.F., BOHOYO, F., HERNÁNDEZ-MOLINA, F.J., CASAS, D., GALINDO-ZALDÍVAR, J., RUANO, P. & MALDONADO, A. (2016) Tectonic Activity Evolution of the Scotia-Antarctic Plate Boundary from Mass Transport Deposit Analysis. *Journal of Geophysical Research: Solid Earth*, **121,** 2216-2234.

PÉREZ, L.F., MALDONADO, A., HERNÁNDEZ-MOLINA, F.J., LODOLO, E., BOHOYO, F. & GALINDO-ZALDÍVAR, J. (2017) Tectonic and Oceanographic Control of Sedimentary Patterns in a Small Oceanic Basin: Dove Basin (Scotia Sea, Antarctica). *Basin Research*, **29,** 255-276.

PICKERING, K.T., HISCOTT, R.N. & HEIN, F.J. (1989) *Deep-Marine Environments: Clastic Sedimentation and Tectonics*. Allen & Unwin Australia.

POULSEN, C.J., BARRON, E.J., ARTHUR, M.A. & PETERSON, W.H. (2001) Response of the Mid-Cretaceous Global Oceanic Circulation to Tectonic and Co2 Forcings. *Paleoceanography and Paleoclimatology*, **16,** 576-592.

POWELL, C.M., ROOTS, S. & VEEVERS, J. (1988) Pre-Breakup Continental Extension in East Gondwanaland and the Early Opening of the Eastern Indian Ocean. *Tectonophysics*, **155,** 261-283.

PUCÉAT, E., LÉCUYER, C. & REISBERG, L. (2005) Neodymium Isotope Evolution of Nw Tethyan Upper Ocean Waters Throughout the Cretaceous. *Earth and Planetary Science Letters*, **236,** 705-720.

REBESCO, M., HERNÁNDEZ-MOLINA, F.J., VAN ROOIJ, D. & WÅHLIN, A. (2014) Contourites and Associated Sediments Controlled by Deep-Water Circulation Processes: State-of-the-Art and Future Considerations. *Marine Geology*, **352,** 111-154.

REED, D.L., MEYER, A.W., SILVER, E.A. & PRASETYO, H. (1987) Contourite Sedimentation in an Intraoceanic Forearc System: Eastern Sunda Arc, Indonesia. *Marine Geology*, **76,** 223-241.

RICHARDSON, S.E.J., DAVIES, R.J., ALLEN, M.B. & GRANT, S.F. (2011) Structure and Evolution of Mass Transport Deposits in the South Caspian Basin, Azerbaijan. *Basin Research*, **23,** 702-719.

ROMANS, B.W., NORMARK, W.R., MCGANN, M.M., COVAULT, J.A. & GRAHAM, S.A. (2009) Coarse-Grained Sediment Delivery and Distribution in the Holocene Santa Monica Basin, California: Implications for Evaluating Source-to-Sink Flux at Millennial Time Scales. *Geological Society of America Bulletin*, **121,** 1394-1408.

ROMERO-OTERO, G.A., SLATT, R.M. & PIRMEZ, C. (2010) Detached and Shelf-Attached Mass Transport Complexes on the Magdalena Deepwater Fan. In: *Submarine Mass Movements and Their Consequences* (Ed. by D. C. Mosher, C. Shipp, L. Moscardelli, J. D. Chaytor, C. D. P. Baxter, H. J. Lee & R. Urgeles), 593-606. Springer, Dordrecth.

ROMINE, K., DURRANT, J., CATHRO, D. & BERNARDEL, G. (1997) Petroleum Play Element Prediction for the Cretaceous–Tertiary Basin Phase, Northern Carnarvon Basin. *APPEA*, **37,** 315-339.

SALLES, T., MARCHÈS, E., DYT, C., GRIFFITHS, C., HANQUIEZ, V. & MULDER, T. (2010) Simulation of the Interactions between Gravity Processes and Contour Currents on the Algarve Margin (South Portugal) Using the Stratigraphic Forward Model Sedsim. *Sedimentary Geology*, **229,** 95-109.

SCARSELLI, N., MCCLAY, K. & ELDERS, C. (2013). *Submarine Slide and Slump Complexes, Exmouth Plateau, Nw Shelf of Australia*. The Sedimentary Basins of Western Australia IV: Proceedings of the Petroleum Exploration Society of Australia Symposium, Perth.

SCARSELLI, N., MCCLAY, K. & ELDERS, C. (2016) Seismic Geomorphology of Cretaceous Megaslides Offshore Namibia (Orange Basin): Insights into Segmentation and Degradation of Gravity-Driven Linked Systems. *Marine and Petroleum Geology*, **75,** 151-180.

SCHER, H.D. & MARTIN, E.E. (2006) Timing and Climatic Consequences of the Opening of Drake Passage. *science*, **312,** 428-430.

SCHWENK, T. & SPIEß, V. (2009) Architecture and Stratigraphy of the Bengal Fan as Response to Tectonic and Climate Revealed from High-Resolution Seismic Data. *External Controls on Deep-Water Depositional Systems. Special Publication-SEPM (Society of Sedimentary Geologists)*, **92,** 107-131.

945 SETON, M., MÜLLER, R., ZAHIROVIC, S., GAINA, C., TORSVIK, T., SHEPHARD, G., TALSMA, A., GURNIS, M., TURNER,
946 M. & MAUS, S. (2012) Global Continental and Ocean Basin Reconstructions since 200 Ma.
947 *Earth-Science Reviews*, **113,** 212-270.
948 SHANMUGAM, G. (2003) Deep-Marine Tidal Bottom Currents and Their Reworked Sands in Modern
949 and Ancient Submarine Canyons. *Marine and Petroleum Geology*, **20,** 471-491.
950 SINHA, D.K., SINGH, A.K. & TIWARI, M. (2006) Palaeoceanographic and Palaeoclimatic History of Odp
951 Site 763a (Exmouth Plateau), Southeast Indian Ocean: 2.2 Ma Record of Planktic
952 Foraminifera. *Current Science***,** 1363-1369.
953 SMITH, R.L., HUYER, A., GODFREY, J.S. & CHURCH, J.A. (1991) The Leeuwin Current Off Western Australia,
954 1986–1987. *Journal of Physical Oceanography*, **21,** 323-345.
955 SOARES, D.M., ALVES, T.M. & TERRINHA, P. (2014) Contourite Drifts on Early Passive Margins as an
956 Indicator of Established Lithospheric Breakup. *Earth and Planetary Science Letters*, **401,** 116-
957 131.
958 SØMME, T.O., PIPER, D.J., DEPTUCK, M.E. & HELLAND-HANSEN, W. (2011) Linking Onshore–Offshore
959 Sediment Dispersal in the Golo Source-to-Sink System (Corsica, France) During the Late
960 Quaternary. *Journal of Sedimentary Research*, **81,** 118-137.
961 SPOONER, M.I., DE DECKKER, P., BARROWS, T.T. & FIFIELD, L.K. (2011) The Behaviour of the Leeuwin
962 Current Offshore Nw Australia During the Last Five Glacial–Interglacial Cycles. *Global and*
963 *Planetary Change*, **75,** 119-132.
964 STICKLEY, C.E., BRINKHUIS, H., SCHELLENBERG, S.A., SLUIJS, A., RÖHL, U., FULLER, M., GRAUERT, M., HUBER, M.,
965 WARNAAR, J. & WILLIAMS, G.L. (2004) Timing and Nature of the Deepening of the Tasmanian
966 Gateway. *Paleoceanography*, **19**.
967 STOW, D.A. & PIPER, D.J. (1984) Deep-Water Fine-Grained Sediments: Facies Models. *Geological*
968 *Society, London, Special Publications*, **15,** 611-646.

969 STOW, D.A., HERNÁNDEZ-MOLINA, F.J., LLAVE, E., SAYAGO-GIL, M., DÍAZ DEL RÍO, V. & BRANSON, A. (2009)
970 Bedform-Velocity Matrix: The Estimation of Bottom Current Velocity from Bedform
971 Observations. *Geology*, **37,** 327-330.
972 SVENSEN, H., PLANKE, S., MALTHE-SØRENSSEN, A., JAMTVEIT, B., MYKLEBUST, R., EIDEM, T.R. & REY, S.S. (2004)
973 Release of Methane from a Volcanic Basin as a Mechanism for Initial Eocene Global
974 Warming. *Nature*, **429,** 542.
975 SYMONS, W.O., SUMNER, E.J., TALLING, P.J., CARTIGNY, M.J. & CLARE, M.A. (2016) Large-Scale Sediment
976 Waves and Scours on the Modern Seafloor and Their Implications for the Prevalence of
977 Supercritical Flows. *Marine Geology*, **371,** 130-148.
978 TCHERNIA, P. (1980) *Descriptive Regional Oceanography*. Pergamon.
979 THÖLE, H., KUHLMANN, G., LUTZ, R. & GAEDICKE, C. (2016) Late Cenozoic Submarine Slope Failures in the
980 Southern North Sea–Evolution and Controlling Factors. *Marine and Petroleum Geology*, **75,**
981 272-290.
982 TINDALE, K., NEWELL, N., KEALL, J. & SMITH, N. (1998) Structural Evolution and Charge History of the
983 Exmouth Sub-Basin, Northern Carnarvon Basin, Western Australia. In: *The Sedimentary*
984 *Basins of Western Australia 2: Proceedings of the Petroleum Exploration Society of Australia*
985 (Ed. by P. G. Purcell & R. R. Purcell), 473-490, Perth.
986 TOURNADOUR, E., MULDER, T., BORGOMANO, J., HANQUIEZ, V., DUCASSOU, E. & GILLET, H. (2015) Origin and
987 Architecture of a Mass Transport Complex on the Northwest Slope of Little Bahama Bank
988 (Bahamas): Relations between Off-Bank Transport, Bottom Current Sedimentation and
989 Submarine Landslides. *Sedimentary Geology*, **317,** 9-26.
990 UENZELMANN-NEBEN, G. (2002) Contourites on the Agulhas Plateau, Sw Indian Ocean: Indications for
991 the Evolution of Currents since Palaeogene Times. *Geological Society, London, Memoirs*, **22,**
992 271-288.

993 UENZELMANN-NEBEN, G. (2006) Depositional Patterns at Drift 7, Antarctic Peninsula: Along-Slope
994 Versus Down-Slope Sediment Transport as Indicators for Oceanic Currents and Climatic
995 Conditions. *Marine geology*, **233,** 49-62.
996 UENZELMANN-NEBEN, G. & GOHL, K. (2012) Amundsen Sea Sediment Drifts: Archives of Modifications in
997 Oceanographic and Climatic Conditions. *Marine Geology*, **299,** 51-62.
998 VANDORPE, T., VAN ROOIJ, D. & DE HAAS, H. (2014) Stratigraphy and Paleoceanography of a Topography-
999 Controlled Contourite Drift in the Pen Duick Area, Southern Gulf of Cádiz. *Marine Geology*,
1000 **349,** 136-151.
1001 VEEVERS, J., POWELL, C.M. & ROOTS, S. (1991) Review of Seafloor Spreading around Australia. I.
1002 Synthesis of the Patterns of Spreading. *Australian Journal of Earth Sciences*, **38,** 373-389.
1003 VIANA, A., FAUGÈRES, J.-C. & STOW, D. (1998) Bottom-Current-Controlled Sand Deposits—a Review of
1004 Modern Shallow-to Deep-Water Environments. *Sedimentary Geology*, **115,** 53-80.
1005 VINNELS, J.S., BUTLER, R.W., MCCAFFREY, W.D. & PATON, D.A. (2010) Depositional Processes across the
1006 Sinú Accretionary Prism, Offshore Colombia. *Marine and Petroleum Geology*, **27,** 794-809.
1007 VÖLKER, D., GEERSEN, J., BEHRMANN, J.H. & WEINREBE, W.R. (2012) Submarine Mass Wasting Off
1008 Southern Central Chile: Distribution and Possible Mechanisms of Slope Failure at an Active
1009 Continental Margin. In: *Submarine Mass Movements and Their Consequences* (Ed. by, 379-
1010 389. Springer.
1011 WELLS, P.E. & WELLS, G.M. (1994) Large-Scale Reorganization of Ocean Currents Offshore Western
1012 Australia During the Late Quaternary. *Marine Micropaleontology*, **24,** 157-186.
1013 WIJERATNE, S., PATTIARATCHI, C. & PROCTOR, R. (2018) Estimates of Surface and Subsurface Boundary
1014 Current Transport around Australia. *Journal of Geophysical Research: Oceans*.
1015 WOO, M. & PATTIARATCHI, C. (2008) Hydrography and Water Masses Off the Western Australian Coast.
1016 *Deep Sea Research Part I: Oceanographic Research Papers*, **55,** 1090-1104.
1017 WUNSCH, M., BETZLER, C., LINDHORST, S., LÜDMANN, T. & EBERLI, G.P. (2017) Sedimentary Dynamics Along
1018 Carbonate Slopes (Bahamas Archipelago). *Sedimentology*, **64,** 631-657.

WYNN, R.B. & STOW, D.A. (2002) Classification and Characterisation of Deep-Water Sediment Waves. *Marine Geology*, **192,** 7-22.

YOUNG, H.C., LEMON, N.M. & HULL, J. (2001) The Middle Cretaceous to Recent Sequence Stratigraphic Evolution of the Exmouth-Barrow Margin, Western Australia. *The APPEA Journal*, **41,** 381-413.

ZHU, M., GRAHAM, S., PANG, X. & MCHARGUE, T. (2010) Characteristics of Migrating Submarine Canyons from the Middle Miocene to Present: Implications for Paleoceanographic Circulation, Northern South China Sea. *Marine and Petroleum Geology*, **27,** 307-319.

10. Figure Captions

Figure 1. (a) Regional map of the study area, the Exmouth Plateau (EP), to the south of the plate boundary (bold black line), where the Australian Plate subducts beneath the Eurasian Plate. Ocean current pathways are modified from (Wijeratne *et al.*, 2018). (b) Location map of the study area (blue polygon) and the distribution of seismic reflection and well data. The blue polygon defines the total area; the grey lines represent 2D seismic data and the black polygon defines the 3D seismic volume (Duyfken). Wells used in this study are coloured in green. The regional 2D seismic line (in orange) is shown in Figure 3. Abbreviations for the North Carnarvon Sub-basins are as follows: BA: Barrow Sub-basin; BE: Beagle Sub-basin; DA: Dampier Sub-basin; EP: Exmouth Plateau; EX: Exmouth Sub-basin; RP: Rankin Platform; CRFZ: Cape Range Fracture Zone. Abyssal plains are: AR: Argo; GA: Gascoyne; CU: Cuvier. Abbreviations for ocean currents are: LC: Leeuwin Current; LU: Leeuwin Undercurrent; ITF: Indonesian Throughflow; SEC: South Equatorial Current; WAC: West Australian Current; FC: Flinders Current; sSICC: south South Indian Counter Current; ACC: Antarctic Circumpolar Current. Shaded relief GEBCO_2014 bathymetry map downloaded from https://www.ngdc.noaa.gov/maps/autogrid/ (accessed on 20 February 2018, 2.41 pm GMT). Sub-basins outline and topography grid are from Geoscience Australia.

Figure 2. Tectonostratigraphic framework of the Exmouth Plateau modified from Kelman *et al.* (2013), geological time-scale from Gradstein *et al.* (2012), the palaeo-water depth is inferred from Hull and Griffiths (2002), the sea-level curve is from Haq *et al.* (1987), and regional events (tectonic in red, oceanographic in blue, and climatic in green) are compiled from references discussed in the text. Four regional horizons (Horizon A, B, C, and D) are mapped across the study area, which define three seismic units: SU-1, SU-2, and SU-3. Local horizons are mapped within 3D seismic reflection data (Horizon C-1 to C-5). Note that Horizon C-2 is not plotted as it is not sampled by biostratigraphic well (i.e. Orthrus-1).

Figure 3. Regional 2D seismic line across the study area (a) uninterpreted, and (b) interpreted. Four regional horizons (Horizon A-D) have been mapped, which define three seismic units: SU-1, SU-2, and SU-3.

Figure 4. A simplified well correlation panel showing gross lithology distribution and stratigraphic relationships, based on core data (ODP 762) and ditch cuttings (other wells). Datum is Top Muderong Shale (Aptian). See Figure 1b for well locations on map and Figure 3 for well locations on regional seismic section.

Figure 5. General seismic facies characteristics observed in each seismic unit.

Figure 6. Representative seismic sections showing the main seismic facies characteristics of each seismic unit. The location of each seismic line is shown in Figure 7a. Note that line f and g have different scale.

Figure 7. (a) Base map showing the location of seismic sections (Fig. 6), wells and the main present-day bathymetric structural features. (b) Depth structure map of Horizon A. (c-e) Isopach maps (left) and seismic facies map (right) of each seismic unit.

Figure 8. (a) Depth structure map of Horizon A within 3D seismic area. (b) RMS amplitude extraction from Horizon A. Note the slightly curved, mainly straight to very low-sinuosity lineations. The

sinuous lineations (SW area) are roughly parallel to the trend of SU-1 contourite channel (Fig. 6c), and the dominant, NE-SW oriented, straight lineations (central area). (c) Seismic section across the sinuous lineations in Figure 8b showing SU-1 contourite channel. (d) Seismic section across the straight lineations in Figure 8b showing U-shaped depressions interpreted as furrows.

Figure 9. (a) Seismic section across the transition zone into the VFZ; showing sediment waves in cross-section most notably between Horizon C-2 and C-4. (b-d) Shaded relief depth structure maps (left) and interpretive sketches (right) of Horizon C-2, C-3, and C-4.

Figure 10. (a) Close-up image of Horizon C-4. (b) Seismic section across NW-trending channel infilled by NE-dipping reflections, interpreted as a result of bottom (palaeo-WAC) and turbidity currents interaction. Note the basal lineations at the base of the channel.

Figure 11. (a) Detailed strike seismic section of multiple occurrences of MTCs (i.e. MTC-1, 2 and 3) in the Kangaroo Syncline. Variance maps showing (b) lateral margin and remnant blocks within the MTC-1 body, (c) grooves on MTC-2 basal shear surface, and (d) primary and secondary flow fabrics (PFFs and SFFs) on MTC-3 top surface (seabed).

Figure 12. (a) SU-1 palaeo-flow indicators documented in this study (left) with inferred palaeo-flow direction (light blue arrow), and reconstruction of plate configurations with interpreted ocean circulation during Late Cretaceous (from Pucéat *et al.*, 2005). (b) SU-2 palaeo-flow indicators documented in this study (left) with inferred palaeo-flow direction (light blue arrow) and reconstruction of plate configurations with interpreted ocean circulation during middle Eocene (inferred from Barron & Peterson, 1991). Abbreviations are: EP: Exmouth Plateau; DP: Drake Passage; TG: Tasman Gap. Global plate tectonic reconstruction is from Seton *et al.* (2012) with coastline (black) and continent-ocean boundary (blue). Oceanic age data are from (Müller *et al.*, 2013).

1091 Fig. 1

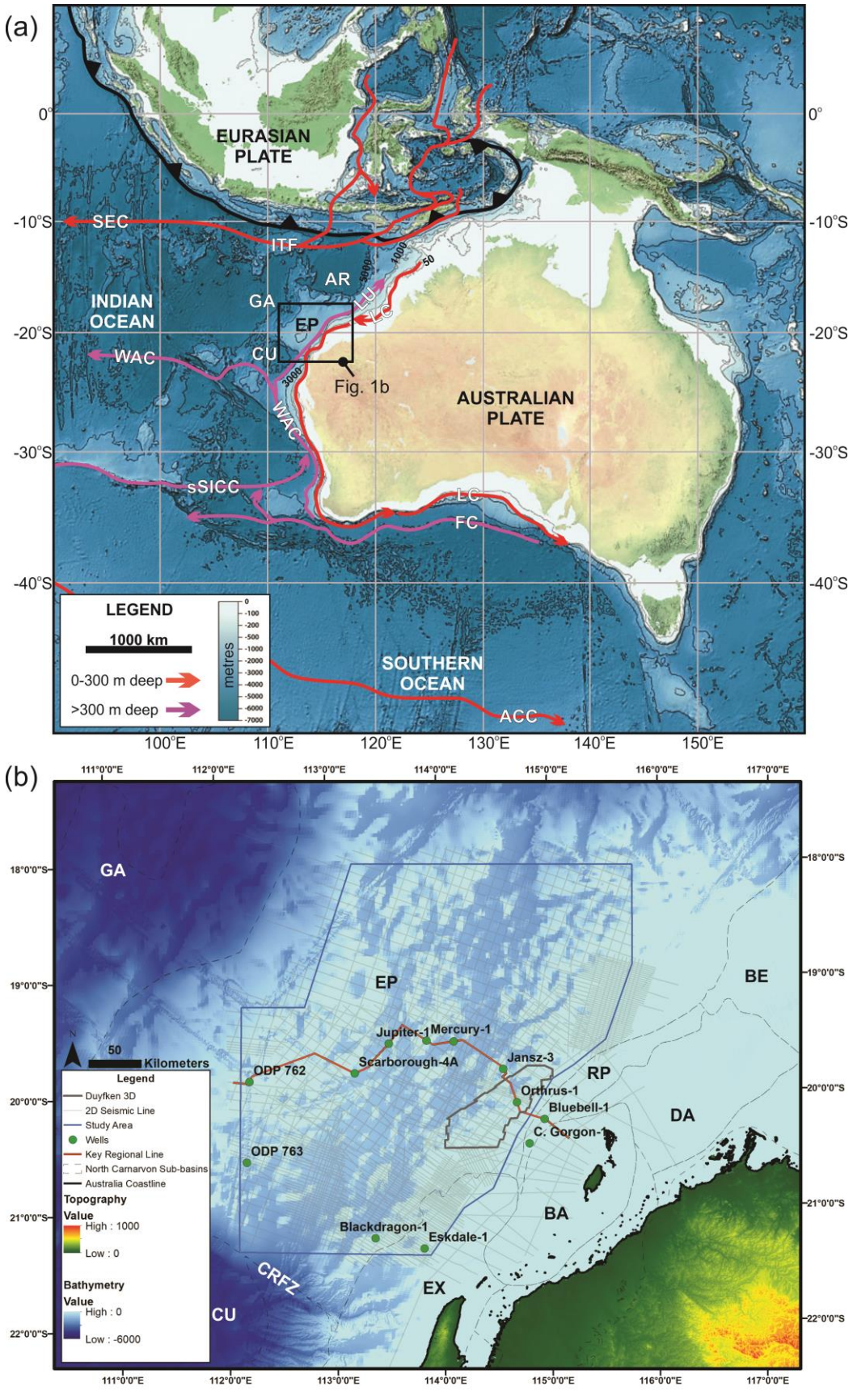

1092

1093 Fig. 2

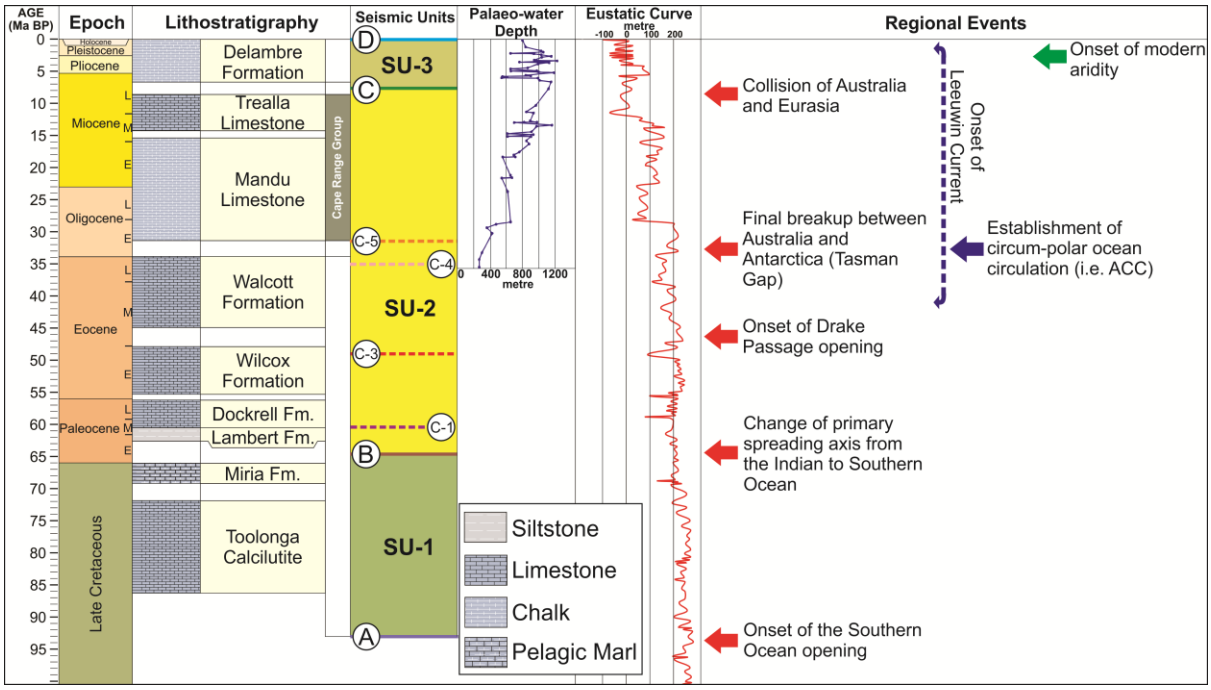

1094

1095

1096 Fig. 3

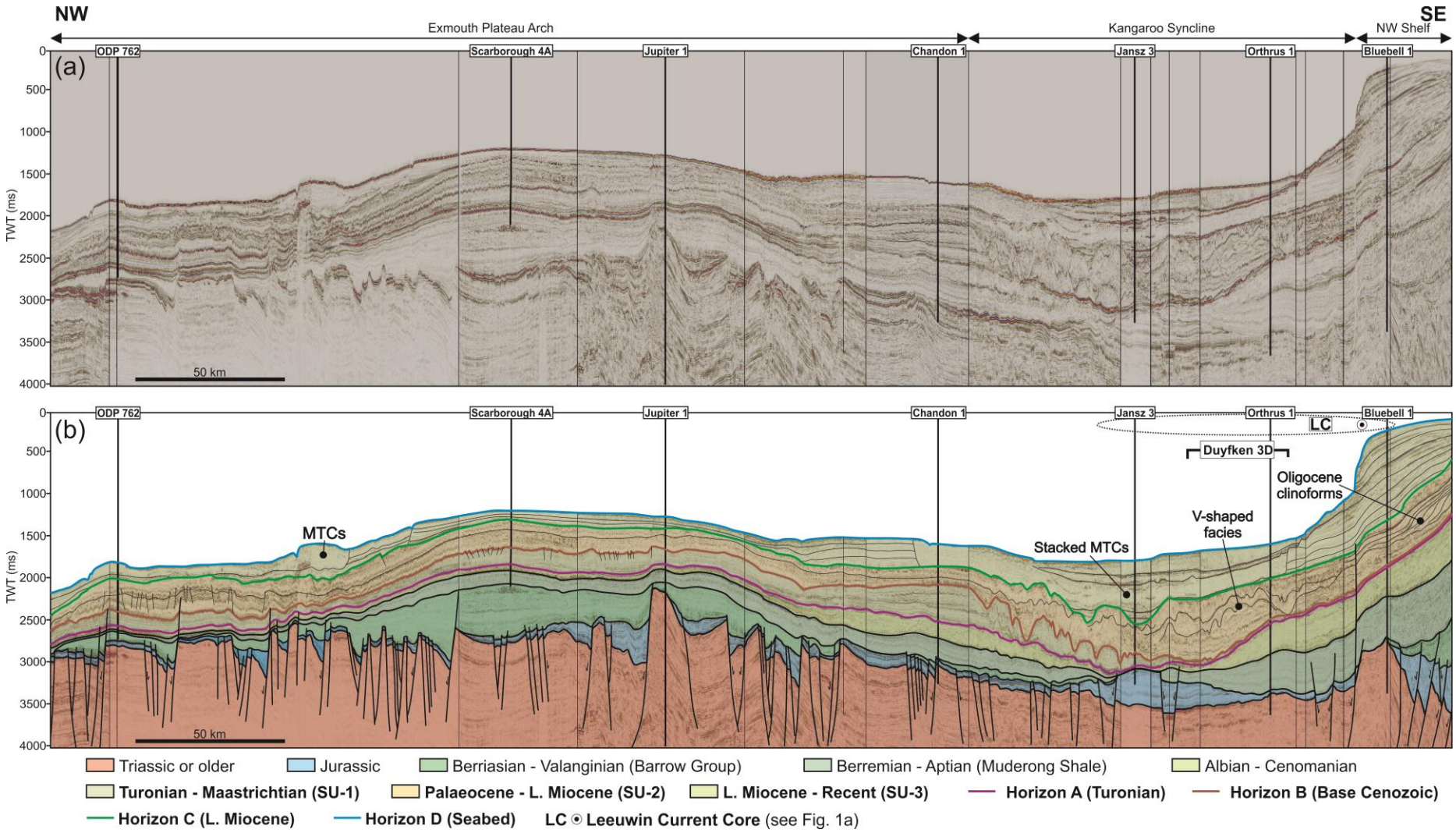

1097

1098 Fig. 4

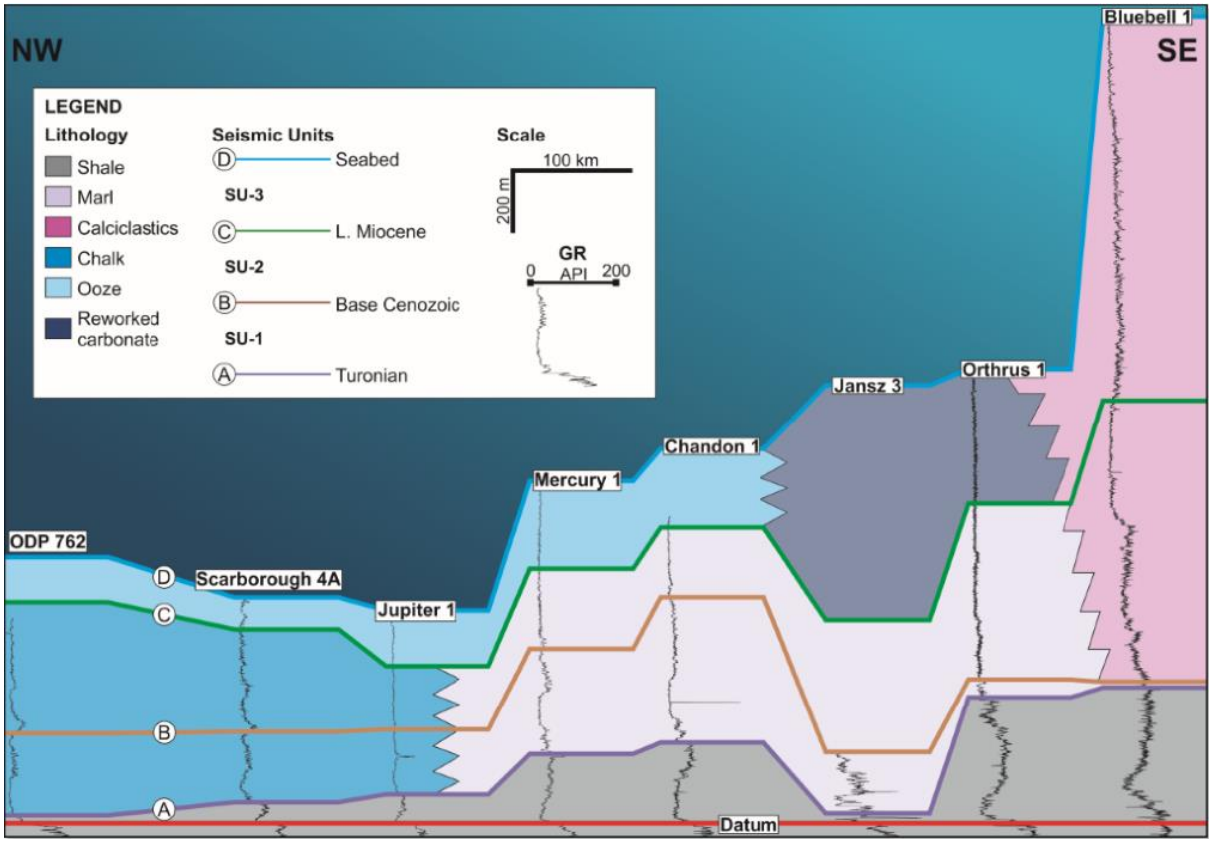

1099

1100 Fig. 5

Facies	Description	Example		Interpretation	Occurrences within SU
SF-1	Sub-parallel, continuous, alternating low- to high-amplitude reflections, local offset faults are common in some places.	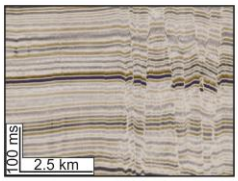	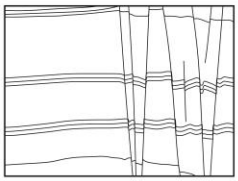	Hemipelagic deposits or sheeted contourite drift (e.g. Faugères et al., 1999).	SU-1 and SU-2: Predominantly in the northern and eastern part of the study area. SU-3: Predominantly around the Exmouth Plateau Arch.
SF-2	Sub-parallel, continuous, alternating low- to high-amplitude with truncated internal reflections. Oriented sub-parallel or oblique with slope in map-view.	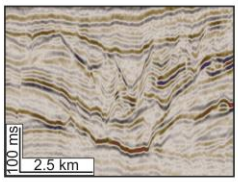	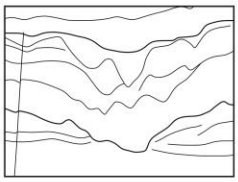	Contourite channel (e.g. Faugères et al., 1999).	SU-1 and SU-2: Predominantly in the eastern part of the study area, along the Kangaroo Syncline.
SF-3	Sub-parallel to wavy, variable low- to high-amplitude, with common v-shaped, internal truncations. Commonly oriented oblique to slope.	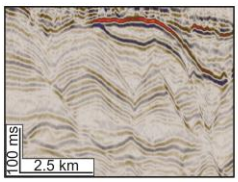	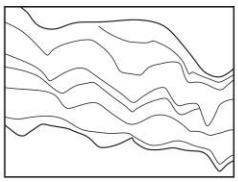	Sediment waves, or erosional remnants of sediment waves (e.g. Faugères et al., 1999).	SU-2: Encountered in the northern part of the Kangaroo Syncline, termed as v-shaped facies zone (VFZ).
SF-4	Discontinuous to chaotic, variable low- to high-amplitude reflections.	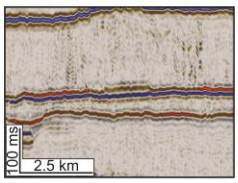	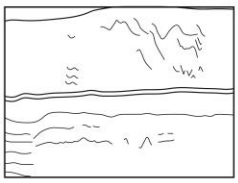	Mass-transport complexes (MTCs) (e.g. Bull et al., 2009)	SU-3: Common in the present-day bathymetric low, such as in the Kangaroo Syncline, and flanks of the Exmouth Plateau Arch.

1101

1102 Fig. 6

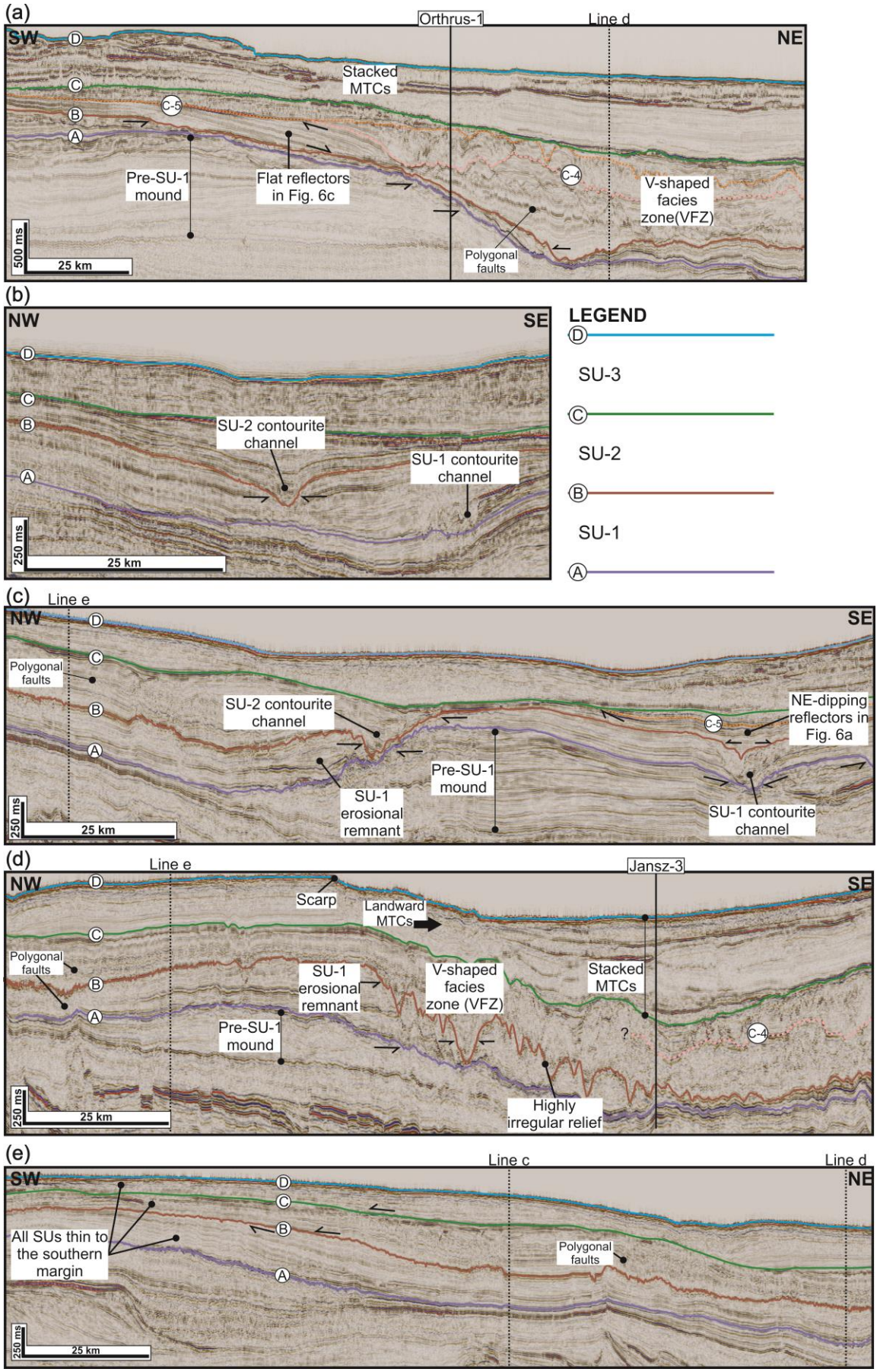

1103

(f)

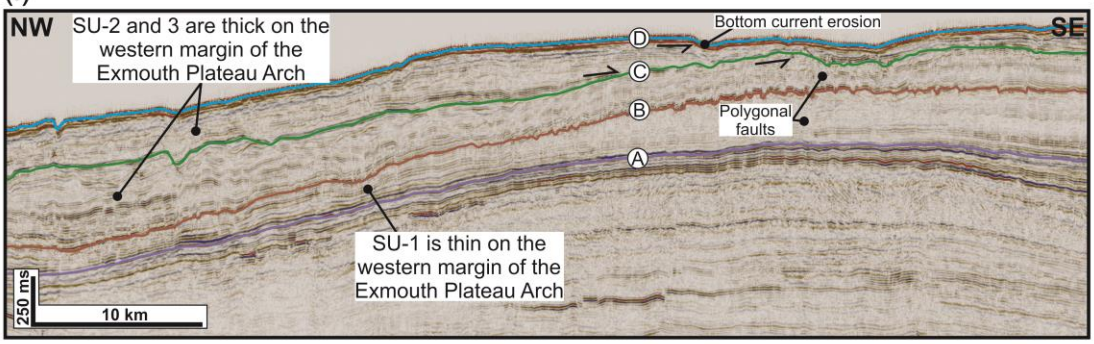
NW
SU-2 and 3 are thick on the western margin of the Exmouth Plateau Arch
Bottom current erosion
SE
D
C
B
A
Polygonal faults
SU-1 is thin on the western margin of the Exmouth Plateau Arch
250 ms
10 km

(g)

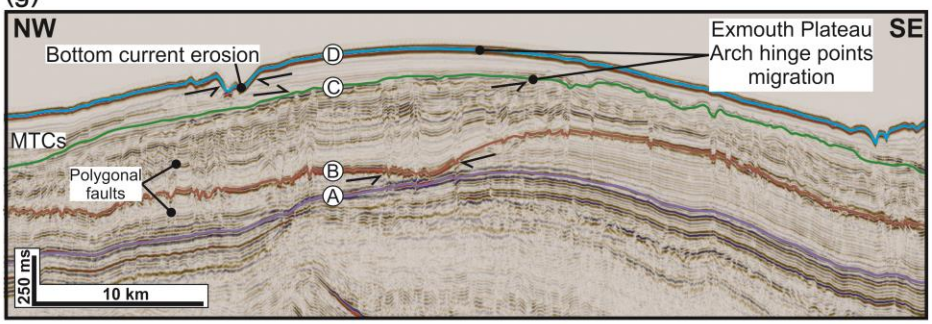
NW
Bottom current erosion
D
C
Exmouth Plateau Arch hinge points migration
SE
MTCs
Polygonal faults
B
A
250 ms
10 km

(h)

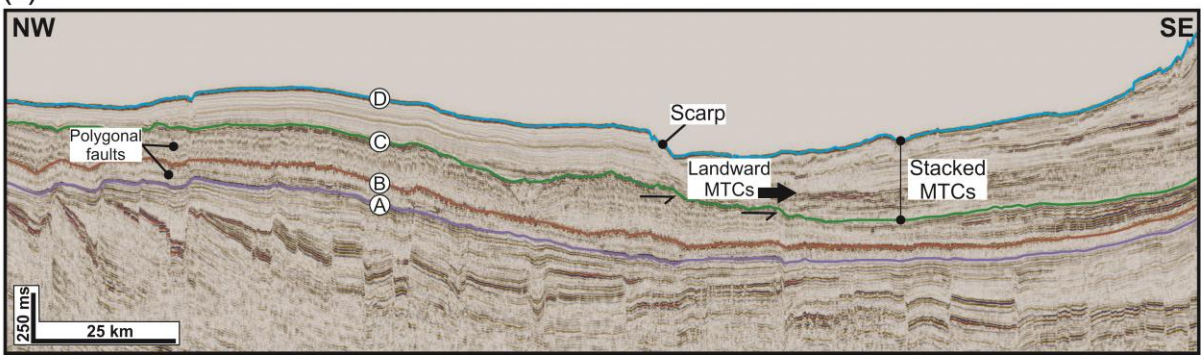
NW
SE
D
C
B
A
Polygonal faults
Scarp
Landward MTCs
Stacked MTCs
250 ms
25 km

1104

1105 Fig. 7

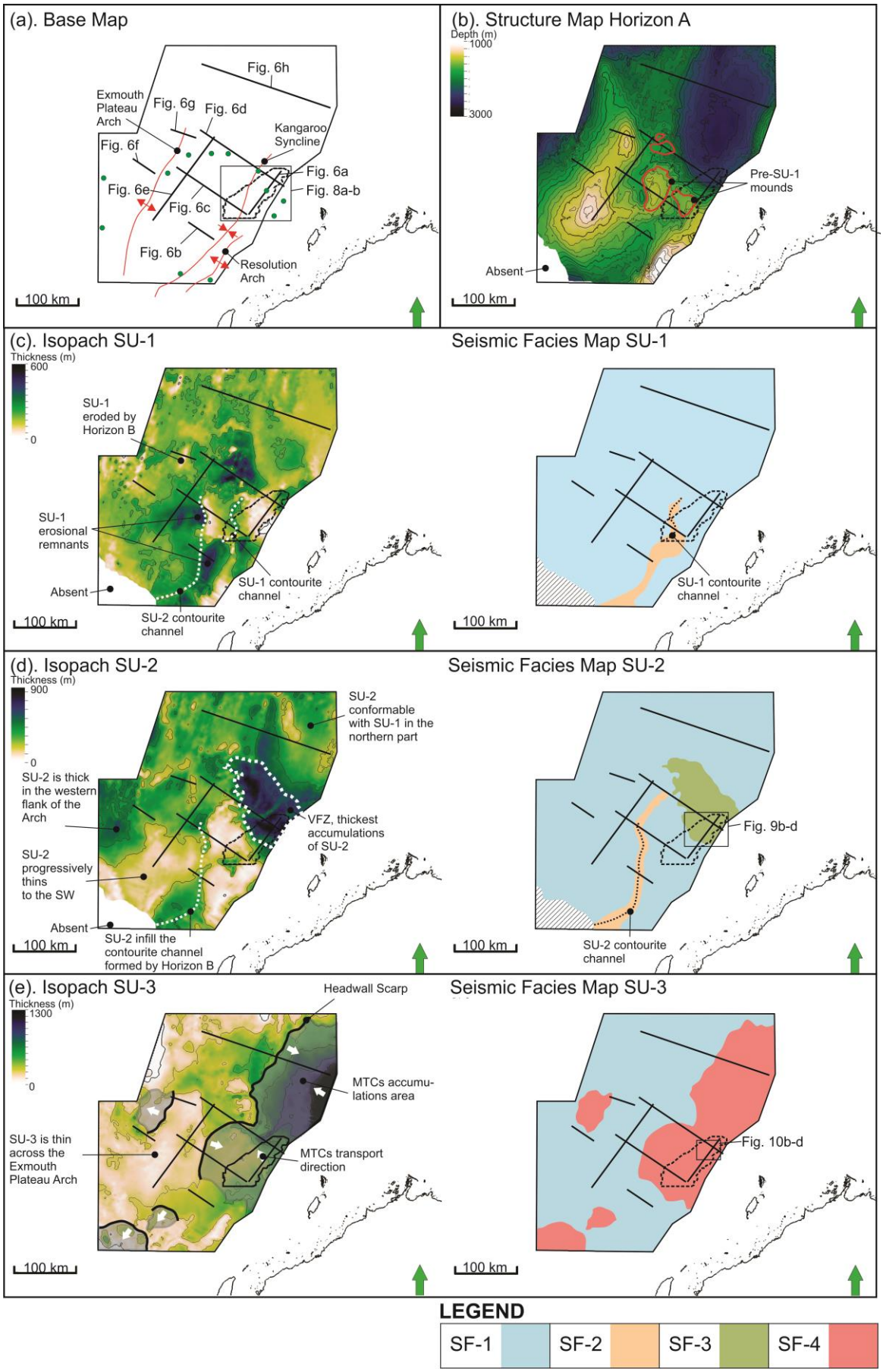

1106

1107 Fig. 8

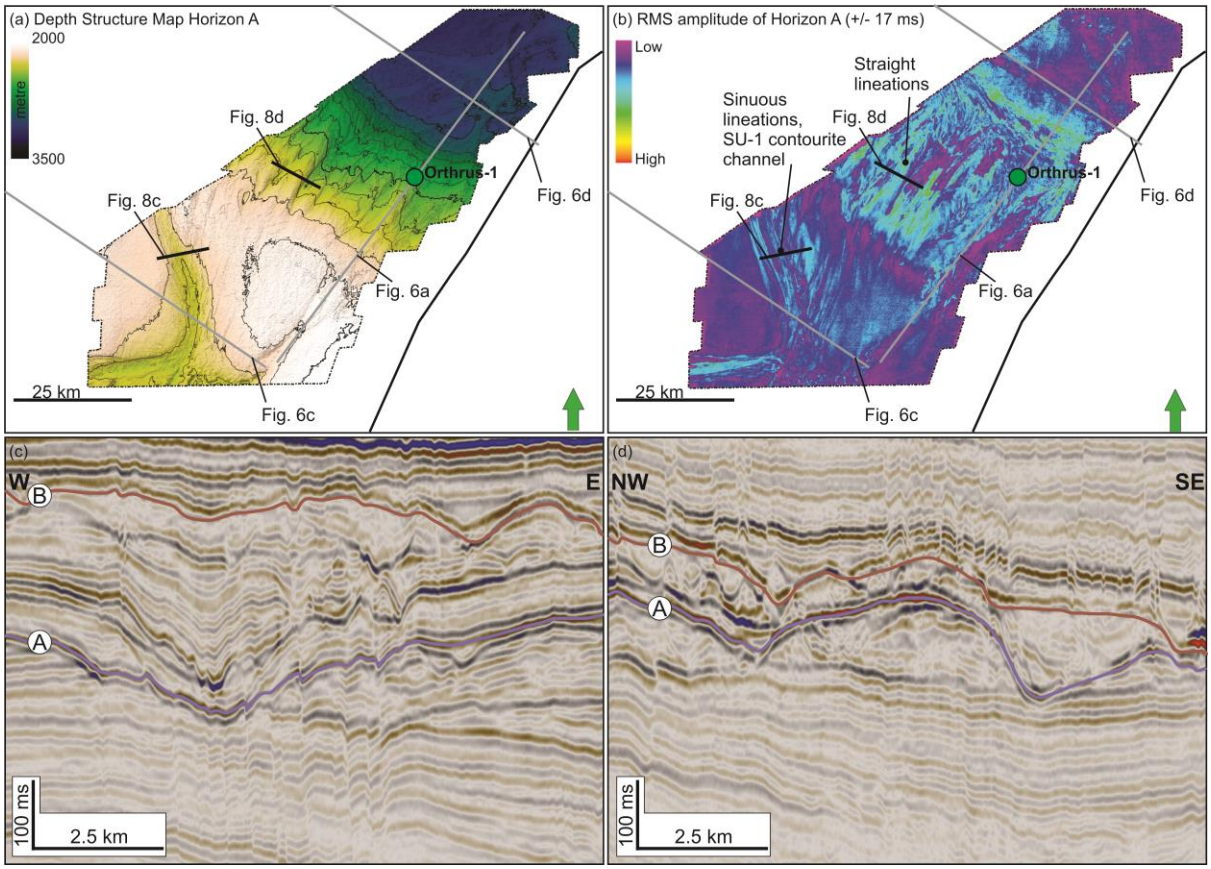

1108

1109 Fig. 9

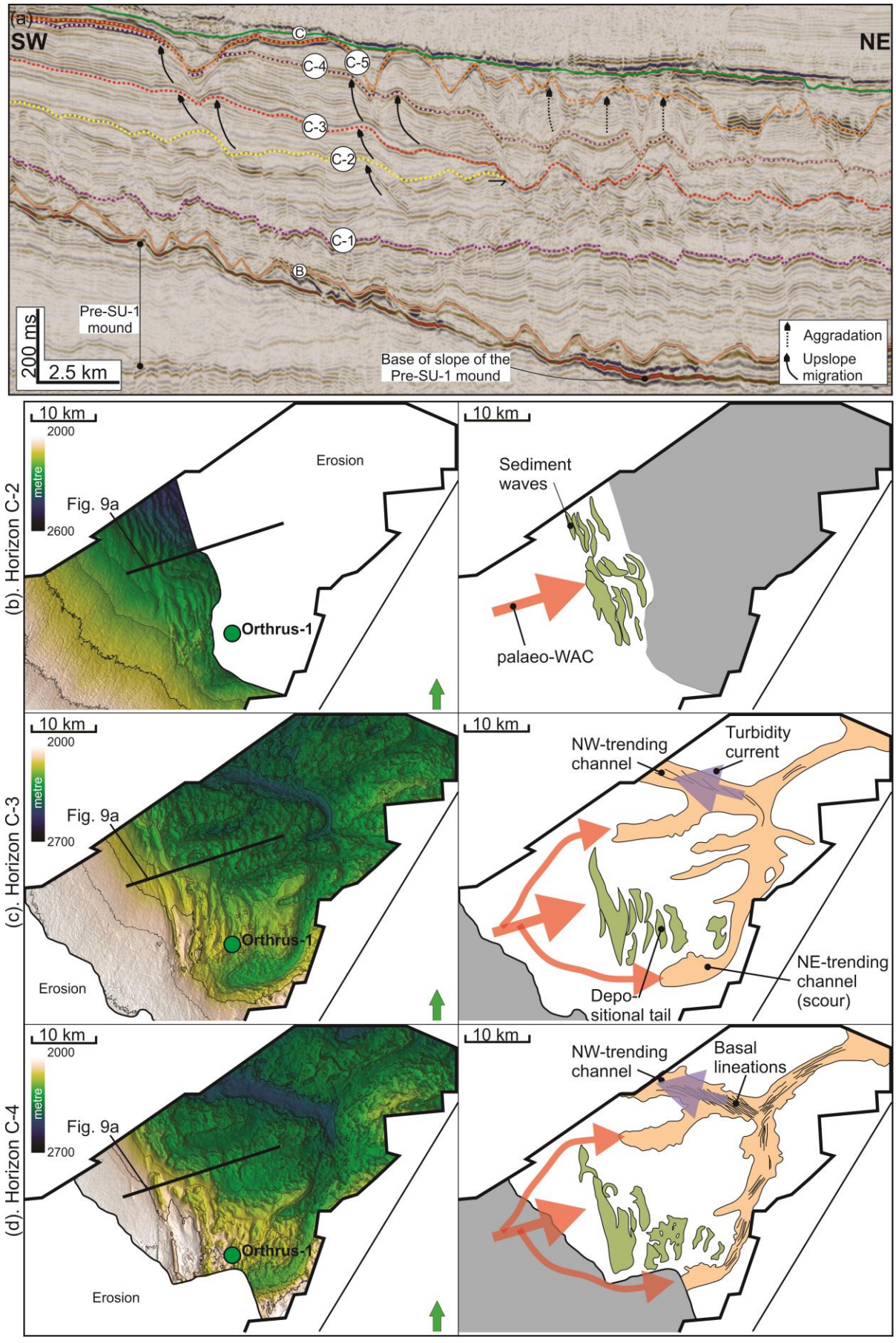

1110

1111 Fig. 10

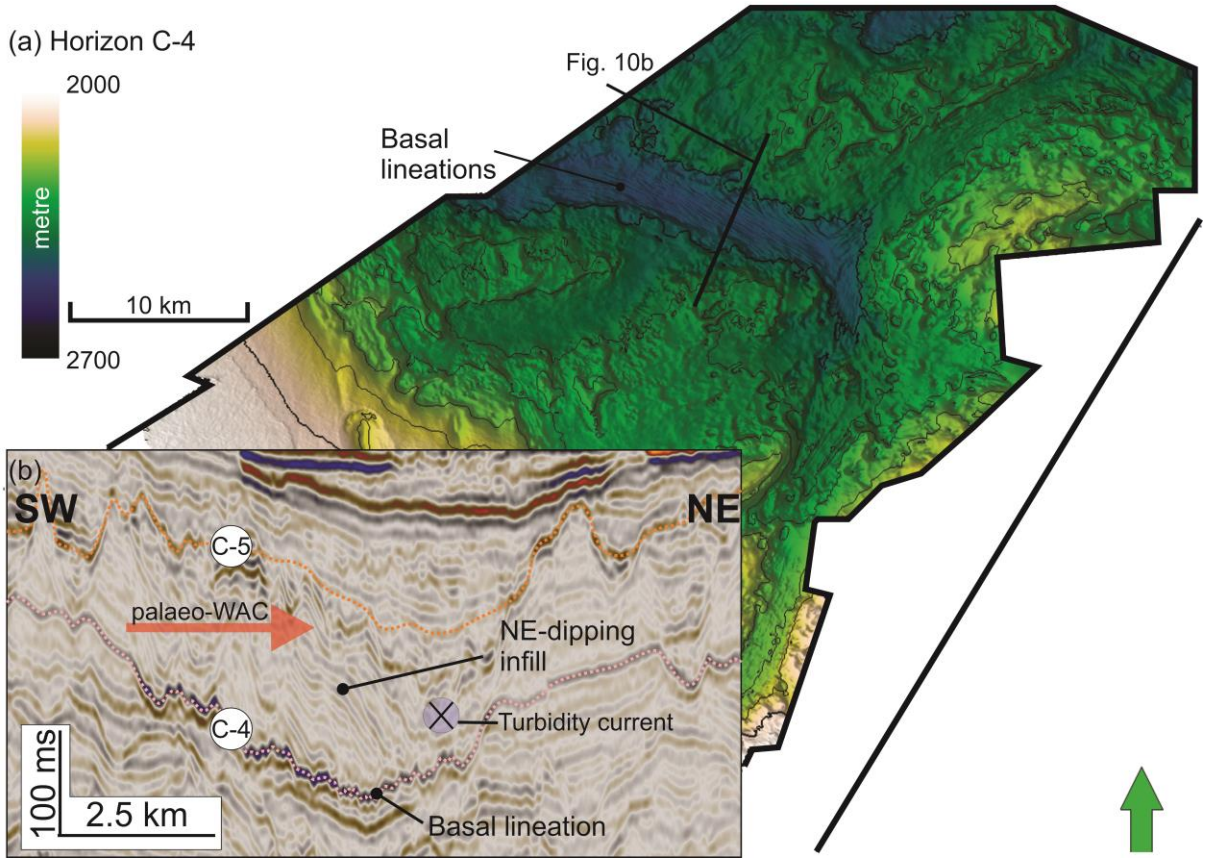

1112

1113 Fig. 11

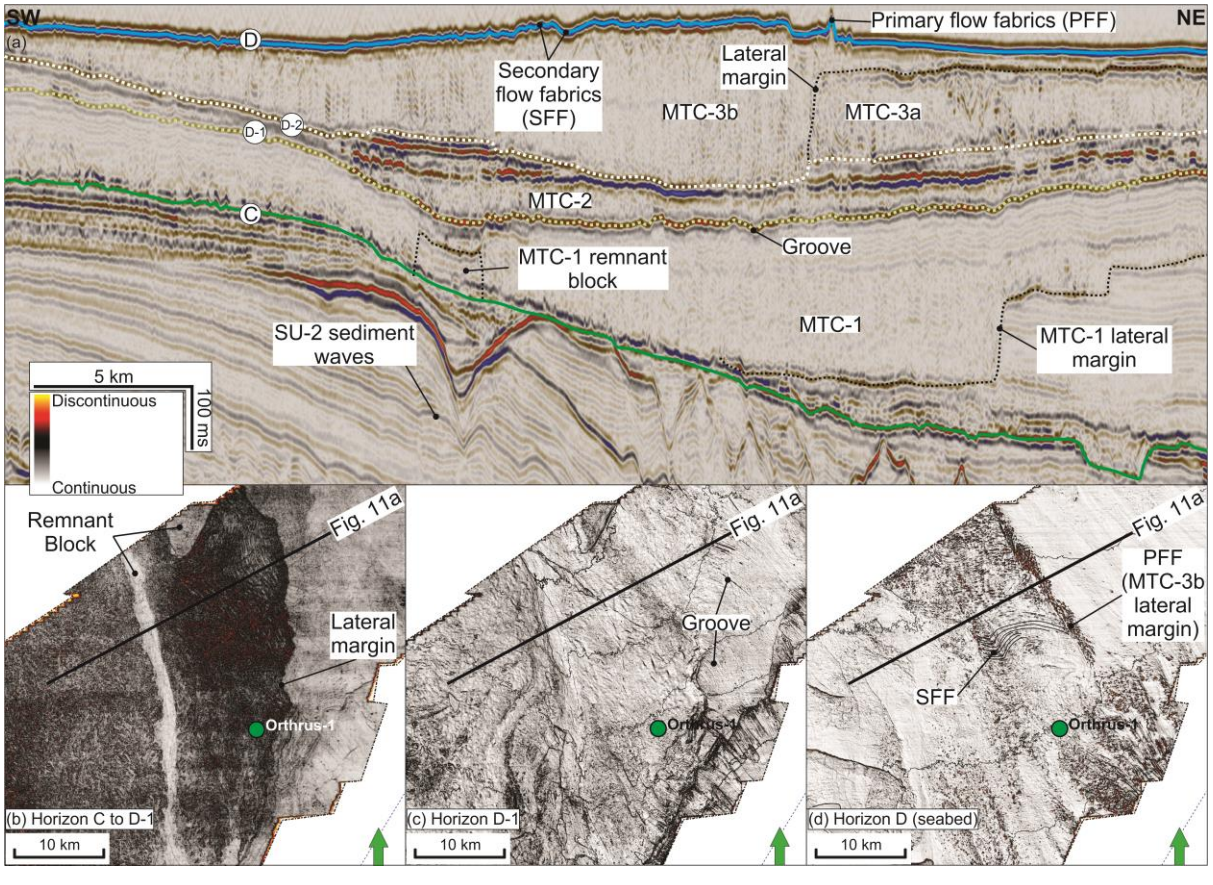

1114

1115 Fig. 12

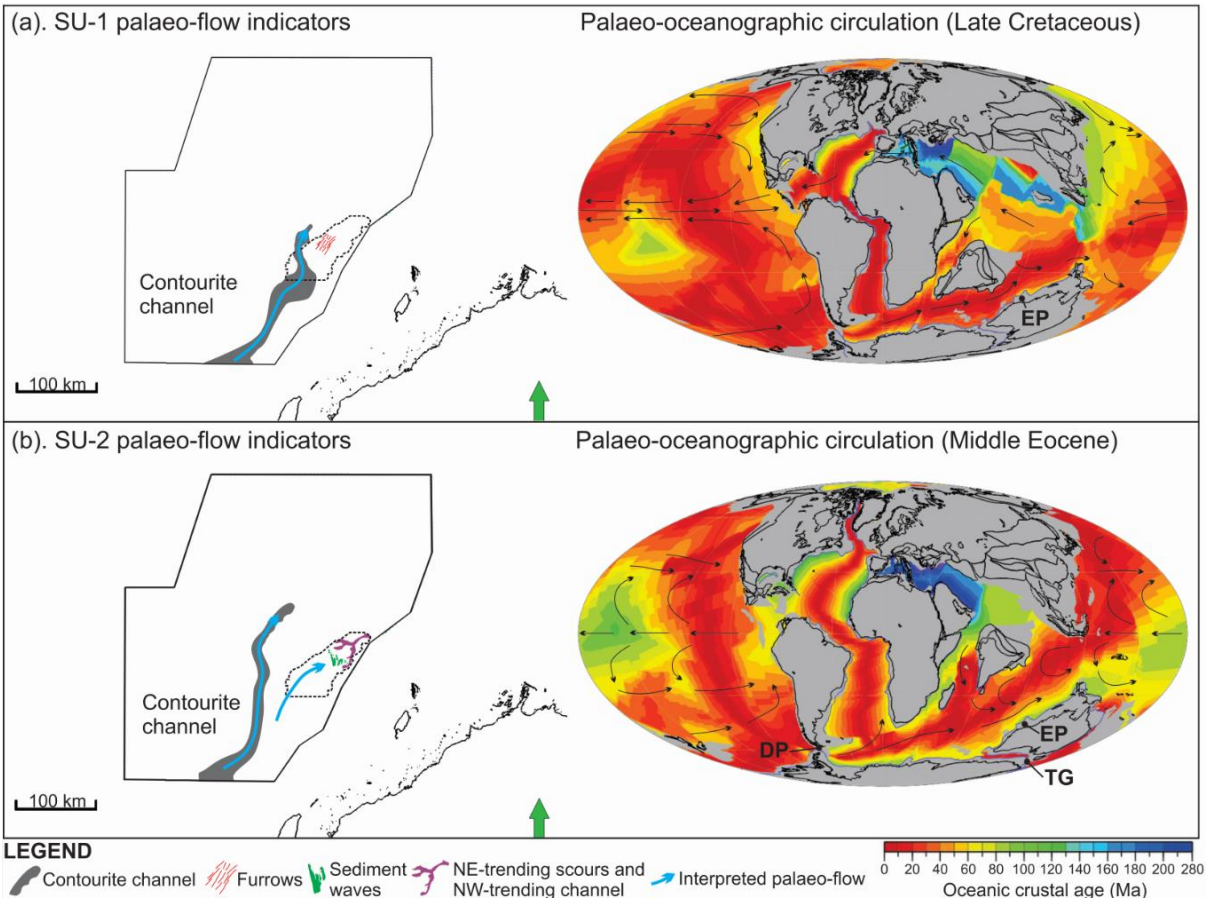

1116